CWP-534

Effective attenuation anisotropy of layered media

Yaping Zhu, Ilya Tsvankin, and Ivan Vasconcelos
Center for Wave Phenomena, Department of Geophysics,
Colorado School of Mines, Golden, CO 80401-1887

ABSTRACT

One of the main factors responsible for effective anisotropy of seismic attenuation is interbedding of thin attenuative layers with different properties. Here, we apply Backus averaging to obtain the complex stiffness matrix for an effective medium formed by an arbitrary number of anisotropic, attenuative constituents. Unless the intrinsic attenuation is uncommonly strong, the effective velocity function is controlled by the real-valued stiffnesses (i.e., is independent of attenuation) and can be determined from the known equations for purely elastic media. Analysis of effective attenuation is more complicated because the attenuation parameters are influenced by coupling between the real and imaginary parts of the stiffness matrix.

The main focus of this work is on effective VTI (transversely isotropic with a vertical symmetry axis) models that include isotropic and VTI constituents. Assuming that the stiffness contrasts, as well as the intrinsic velocity and attenuation anisotropy, are weak, we develop explicit first-order (linear) and second-order (quadratic) approximations for the attenuation-anisotropy parameters ϵ_Q, δ_Q, and γ_Q. Whereas the first-order approximation for each parameter is given simply by the volume-weighted average of its interval values, the second-order terms reflect the coupling between various factors related to both heterogeneity and intrinsic anisotropy. Interestingly, the effective attenuation for P- and SV-waves is anisotropic even for a medium composed of isotropic layers with no attenuation contrast, provided there is a velocity variation among the constituent layers. Contrasts in the intrinsic attenuation, however, do not create attenuation anisotropy, unless they are accompanied by velocity contrasts.

Extensive numerical testing shows that the second-order approximation for ϵ_Q, δ_Q, and γ_Q is close to the exact solution for most plausible subsurface models. The accuracy of the first-order approximation depends on the magnitude of the quadratic terms, which is largely governed by the strength of the velocity (rather than attenuation) contrasts and velocity anisotropy. The effective attenuation parameters for multiconstituent VTI models generally exhibit more variation than do the velocity parameters, with almost equal probability of positive and negative values. If some of the constituents are azimuthally anisotropic with misaligned vertical symmetry planes, the effective velocity and attenuation functions may have different symmetries and principal azimuthal directions.

Key words: attenuation, effective attenuation anisotropy, transverse isotropy, layered media, weak-anisotropy approximation

1 INTRODUCTION

The directional dependence of attenuation has been observed in laboratory experiments (e.g., Hosten et al., 1987; Tao and King, 1990; Prasad and Nur, 2003; Zhu et al., 2006) and several field case studies (e.g., Lynn et al., 1999; Vasconcelos and Jenner, 2005). While the substantial magnitude of attenuation anisotropy for many subsurface formation is unquestionable, the underlying physical mechanisms are not completely understood.

In their analysis of a shallow multiazimuth reverse VSP survey, Liu et al. (1993) estimated anisotropy in both velocity and attenuation, and attributed it to stress-induced fractures and microcracks. Pointer et al. (2000) discuss three different mechanisms for wave-induced fluid flow in cracked porous media that might result in anisotropic velocities and attenuation coefficients when the cracks are aligned. A poroelastic model introduced by Chapman (2003) in his discussion of frequency-dependent anisotropy can explain strong anisotropic attenuation in the seismic frequency band. Using Chapman's model, Maultzsch et al. (2003) estimated the Q-factor as a function of phase angle for synthetic samples composed of sand-epoxy matrix with embedded thin metal discs. Analysis of seismic body waves and normal-mode data shows that even the inner core of the earth possesses attenuation anisotropy likely caused by columnar crystals elongated in the radial direction (Souriau and Romanowicz, 1996; Bergman, 1997).

Another possible cause of effective attenuation anisotropy is interbedding of thin layers with different attenuation coefficients. Long-wavelength velocity anisotropy of layered media is discussed extensively in the literature (e.g., Backus, 1962; Berryman, 1979; Schoenberg and Muir, 1989; Shapiro and Hubral, 1996; Bakulin, 2003; Bakulin and Grechka, 2003). Although attenuation anisotropy usually accompanies velocity anisotropy (e.g., Tao and King, 1990; Arts and Rasolofosaon, 1992), much less attention has been devoted to studies of effective anisotropy of layered attenuative media. Sams (1995) measured effective attenuation coefficients partially resulting from apparent (layer-induced) attenuation, but his work is restricted to isotropic models. Molotkov and Bakulin (1998) discussed a matrix-averaging technique for stratified lossy porous medium and obtained an effective Biot medium with anisotropic viscosity and relaxation. By employing the correspondence principle (Bland, 1960) for thin-layered viscoelastic media, Carcione (1992) derived the complex stiffnesses of effective media composed of attenuative, isotropic constituent layers. This effective stiffness matrix can be used to quantify both velocity anisotropy and attenuation anisotropy.

Here we analyze the effective properties of a sequence of attenuative *anisotropic* layers. The discussion is focused primarily on transversely isotropic (TI) constituents with a vertical symmetry axis for both velocity and attenuation. First, the Backus averaging technique is used to obtain the exact stiffness matrix in the low-frequency limit. Then we develop the first- and second-order approximations for the effective velocity and attenuation anisotropy in terms of the interval anisotropy parameters and stiffness contrasts. The second-order (quadratic) solution is particularly helpful in evaluating the contributions of various factors to the effective attenuation-anisotropy parameters. Numerical tests demonstrate that the performance of the approximations is mostly influenced by the velocity field (i.e., by the real parts of the stiffness coefficients). Simulations for a representative set of random layered TI models allow us to estimate the bounds on the effective velocity and attenuation parameters. Finally, we consider azimuthally anisotropic constituent layers and discuss the possibility of misaligned symmetry directions for the velocity and attenuation functions.

2 EFFECTIVE PARAMETERS OF LAYERED ANISOTROPIC ATTENUATIVE MEDIA

The Backus (1962) averaging technique was originally introduced to compute the effective properties of a stack of elastic (non-attenuative) isotropic layers in the long-wavelength limit. Here, we derive the effective stiffness coefficients for stratified models composed of thin attenuative anisotropic layers.

The constitutive relationship for attenuative media can be expressed in the time domain as

$$\tau = \mathcal{L}\mathbf{e}\,, \tag{1}$$

where τ and $\mathbf{e}$ are the real-valued stress and strain tensors, respectively. $\mathcal{L}$ is a first-order linear differential operator that reduces to the real-valued stiffness tensor for elastic media. For example, consider a 1-D standard linear solid model (also called the Zener model) used to characterize dissipative rocks and polymers (e.g., Ferry, 1980; Carcione, 2001). This model includes a spring combined with a unit consisting of another spring and a dashpot connected in parallel; its viscoelastic behavior is described by

$$\tau + \tau_\tau \partial_t \tau = M_R(\epsilon + \tau_e \partial_t e)\,, \tag{2}$$

where τ_τ and τ_e are the two relaxation times for the mechanical system, and M_R is the "relaxed" modulus. For elastic media, the relaxation times vanish, and M_R reduces to a real-valued modulus.

Transforming the constitutive relationship from equation 1 into the frequency domain yields

$$\tilde{\tau} = \tilde{C}\,\tilde{e}\,, \tag{3}$$

where all quantities become complex-valued (denoted by $\tilde{}$); $\tilde{C}$ is the complex stiffness tensor.

Suppose a thin-layered model includes N types of constituents, whose spatial distribution is stationary across all the layers. For simplicity, throughout the paper the layering plane is assumed to be horizontal. The medium properties are constant within each layer but change across layer boundaries (medium interfaces). Different layers belong to the same constituent if they have identical medium properties including both velocity and attenuation. For example, it is possible to form a model with hundreds of thin layers by using just two interbedding constituents.

The Backus averaging technique for both elastic and attenuative media is applied in the long-wavelength limit, which means that the dominant wavelength is much larger than the thickness of all layers. Following Backus (1962) and Schoenberg and Muir (1989), we assume that in the time domain the components of the traction vector that acts across interfaces are the same for all layers:

$$\tau_{13}^{(k)} \equiv \tau_{13}\,, \quad \tau_{23}^{(k)} \equiv \tau_{23}\,, \quad \tau_{33}^{(k)} \equiv \tau_{33}\,, \tag{4}$$

where the superscript denotes the k-th constituent. The in-plane strain components are also supposed to be the same:

$$e_{11}^{(k)} \equiv e_{11}\,, \quad e_{22}^{(k)} \equiv e_{22}\,, \quad e_{12}^{(k)} \equiv e_{12}\,. \tag{5}$$

Equations 4 and 5 remain valid for the frequency-domain counterparts of the stress and strain elements:

$$\tilde{\tau}_{13}^{(k)} \equiv \tilde{\tau}_{13}\,, \quad \tilde{\tau}_{23}^{(k)} \equiv \tilde{\tau}_{23}\,, \quad \tilde{\tau}_{33}^{(k)} \equiv \tilde{\tau}_{33}\,, \tag{6}$$

and

$$\tilde{e}_{11}^{(k)} \equiv \tilde{e}_{11}\,, \quad \tilde{e}_{22}^{(k)} \equiv \tilde{e}_{22}\,, \quad \tilde{e}_{12}^{(k)} \equiv \tilde{e}_{12}\,. \tag{7}$$

When the frequency goes to zero, the imaginary parts of the complex stiffness components vanish, and the medium becomes non-attenuative.

Since all stress and strain components in equations 6 and 7 are just the complex counterparts of the corresponding quantities in equations 4 and 5, the effective stiffnesses for layered attenuative media can be obtained using the results of Schoenberg and Muir (1989) for purely elastic models:

$$\tilde{\mathbf{C}}_{NN} = \langle \tilde{\mathbf{C}}_{NN}^{-1} \rangle^{-1}\,, \tag{8}$$

$$\tilde{\mathbf{C}}_{TN} = \langle \tilde{\mathbf{C}}_{TN} \tilde{\mathbf{C}}_{NN}^{-1} \rangle \tilde{\mathbf{C}}_{NN}\,, \tag{9}$$

$$\begin{aligned}\tilde{\mathbf{C}}_{TT} = \langle \tilde{\mathbf{C}}_{TT} \rangle - \langle \tilde{\mathbf{C}}_{TN} \tilde{\mathbf{C}}_{NN}^{-1} \tilde{\mathbf{C}}_{NT} \rangle \\ + \langle \tilde{\mathbf{C}}_{TN} \tilde{\mathbf{C}}_{NN}^{-1} \rangle \tilde{\mathbf{C}}_{NN} \langle \tilde{\mathbf{C}}_{NN}^{-1} \tilde{\mathbf{C}}_{NT} \rangle\,,\end{aligned} \tag{10}$$

where $\langle \cdot \rangle$ denotes the volume-weighted average. The submatrices for each constituent have the following form:

$$\tilde{\mathbf{C}}_{NN}^{(k)} = \begin{bmatrix} \tilde{c}_{33} & \tilde{c}_{34} & \tilde{c}_{35} \\ \tilde{c}_{34} & \tilde{c}_{44} & \tilde{c}_{45} \\ \tilde{c}_{35} & \tilde{c}_{45} & \tilde{c}_{55} \end{bmatrix}, \tag{11}$$

$$\tilde{\mathbf{C}}_{TN}^{(k)} = \tilde{\mathbf{C}}_{NT}^{(k)T} = \begin{bmatrix} \tilde{c}_{13} & \tilde{c}_{14} & \tilde{c}_{15} \\ \tilde{c}_{23} & \tilde{c}_{24} & \tilde{c}_{25} \\ \tilde{c}_{36} & \tilde{c}_{46} & \tilde{c}_{56} \end{bmatrix}, \tag{12}$$

and

$$\tilde{\mathbf{C}}_{TT}^{(k)} = \begin{bmatrix} \tilde{c}_{11} & \tilde{c}_{12} & \tilde{c}_{16} \\ \tilde{c}_{12} & \tilde{c}_{22} & \tilde{c}_{26} \\ \tilde{c}_{16} & \tilde{c}_{26} & \tilde{c}_{66} \end{bmatrix}. \tag{13}$$

Equations 8-13 completely describe the effective properties for any number of constituents with arbitrary anisotropy in terms of both velocity and attenuation.

2.1 Effective stiffnesses for TI media

Transversely isotropic (TI) layers (primarily shales and shaly sands) are common for sedimentary basins (Sayers, 1994; Tsvankin, 2005). Here, we consider a layered medium composed of TI constituents with a vertical symmetry axis (VTI) for both velocity and attenuation. Substituting the complex stiffness matrix $\tilde{c}_{ij}$ of the VTI constituent layers (Zhu and Tsvankin, 2006) into equations 8-13 yields an effective attenuative VTI model with five independent complex stiffnesses:

$$\tilde{c}_{11} = \langle \tilde{c}_{11} \rangle - \langle (\tilde{c}_{13})^2/\tilde{c}_{33} \rangle + \langle 1/\tilde{c}_{33} \rangle^{-1} \langle \tilde{c}_{13}/\tilde{c}_{33} \rangle^2\,, \tag{14}$$

$$\tilde{c}_{33} = \langle 1/\tilde{c}_{33} \rangle^{-1}\,, \tag{15}$$

$$\tilde{c}_{13} = \langle 1/\tilde{c}_{33} \rangle^{-1} \langle \tilde{c}_{13}/\tilde{c}_{33} \rangle\,, \tag{16}$$

$$\tilde{c}_{55} = \langle 1/\tilde{c}_{55} \rangle^{-1}\,, \tag{17}$$

$$\tilde{c}_{66} = \langle 1/\tilde{c}_{66} \rangle^{-1}\,; \tag{18}$$

$\tilde{c}_{12} = \tilde{c}_{11} - 2\tilde{c}_{66}$. The effective velocity-anisotropy parameters in Thomsen (1986) notation are obtained using the real parts c_{ij} of the effective stiffnesses from equations 14-18:

$$V_{P0} \equiv \sqrt{\frac{c_{33}}{\rho}}\,, \quad V_{S0} \equiv \sqrt{\frac{c_{55}}{\rho}}\,, \tag{19}$$

$$\epsilon \equiv \frac{c_{11} - c_{33}}{2c_{33}}\,, \tag{20}$$

$$\delta \equiv \frac{(c_{13} + c_{55})^2 - (c_{33} - c_{55})^2}{2c_{33}(c_{33} - c_{55})}\,, \tag{21}$$

$$\gamma \equiv \frac{c_{66} - c_{55}}{2c_{55}}\,, \tag{22}$$

where $\rho = \langle \rho \rangle$ is the volume-averaged density.

To characterize attenuative anisotropy, we employ the effective attenuation-anisotropy parameters defined by Zhu and Tsvankin (2006):

$$\epsilon_Q \equiv \frac{Q_{33} - Q_{11}}{Q_{11}}\,, \tag{23}$$

$$\delta_Q \equiv \frac{\dfrac{Q_{33} - Q_{55}}{Q_{55}} c_{55} \dfrac{(c_{13} + c_{33})^2}{(c_{33} - c_{55})} + 2\dfrac{Q_{33} - Q_{13}}{Q_{13}} c_{13}(c_{13} + c_{55})}{c_{33}(c_{33} - c_{55})}\,, \tag{24}$$

$$\gamma_Q \equiv \frac{Q_{55} - Q_{66}}{Q_{66}}\,, \tag{25}$$

where $Q_{ij} = c_{ij}/c_{ij}^I$ is the quality-factor matrix (no index summation is applied), and c_{ij}^I is the imaginary part of the stiffness $\tilde{c}_{ij}$. The notation of Zhu and Tsvankin

(2006) also includes two reference parameters — the wavenumber-normalized attenuation coefficients for P- and S-waves in the symmetry (vertical) direction:

$$\mathcal{A}_{P0} = Q_{33}\left(\sqrt{1+1/(Q_{33})^2} - 1\right) \approx \frac{1}{2Q_{33}}\,, \tag{26}$$

$$\mathcal{A}_{S0} = Q_{55}\left(\sqrt{1+1/(Q_{55})^2} - 1\right) \approx \frac{1}{2Q_{55}}\,. \tag{27}$$

The normalized attenuation coefficient is defined as $\mathcal{A} \equiv k^I/k$, where k and k^I are the real and imaginary parts of the complex wavenumber $\tilde{k}$. The approximations in equations 26 and 27 are obtained in the weak-attenuation limit by keeping only the linear terms in the inverse components Q_{ii} $(i = 3, 5)$.

3 APPROXIMATE ATTENUATION PARAMETERS OF EFFECTIVE VTI MEDIA

Explicit equations for the effective stiffnesses in terms of the interval parameters have a rather complicated form. Here, we present approximate expressions that help to evaluate the influence of different factors on the anisotropy of the effective medium. The approximations are developed under the assumption of weak intrinsic velocity and attenuation anisotropy, as well as small contrasts in the stiffnesses between different constituents.

Unless the medium is strongly attenuative and has non-negligible dispersion, the influence of the quality-factor elements on phase velocity is of the second order and typically can be ignored (Červený and Pšenčík, 2005; Zhu and Tsvankin, 2006). Hence, the effective velocity-anisotropy parameters remain practically the same as those for the purely elastic model defined by the real parts of the stiffness elements. Since a detailed description of the velocity anisotropy of fine-layered VTI media can be found in Bakulin (2003), the discussion below is focused primarily on the attenuation-anisotropy parameters.

3.1 First-order approximation

Approximate effective parameters can be derived by expanding the exact equations in the small quantities (velocity- and attenuation-anisotropy parameters and the contrasts in the stiffnesses) and neglecting higher-order terms. In the first-order (linear) approximation, the effective value of any anisotropy parameter is equal simply to its volume-weighted average (Bakulin and Grechka, 2003). For example, the linearized parameter ϵ can be written as

$$\epsilon = \langle \epsilon \rangle = \sum_{k=1}^{N} \phi^{(k)} \epsilon^{(k)}\,, \tag{28}$$

where $\phi^{(k)}$ is the volume fraction of each constituent. Similarly, for the attenuation-anisotropy parameter ϵ_Q we have

$$\epsilon_Q = \langle \epsilon_Q \rangle = \sum_{k=1}^{N} \phi^{(k)} \epsilon_Q^{(k)}\,. \tag{29}$$

Evidently, the effective medium properties in the long-wavelength limit are independent of the spatial sequence of the constituents, which can arranged in an arbitrary order.

3.2 Second-order approximation

The second-order approximation for the effective velocity-anisotropy parameters of two-constituent VTI media is given by Bakulin (2003). Here, we present a more general analysis that accounts for attenuation and allows for an arbitrary number of VTI constituents.

The parameters assumed to be small for each constituent k include $\hat{\Delta} c_{33}^{(k)}$, $\hat{\Delta} c_{55}^{(k)}$, $\hat{\Delta} Q_{33}^{(k)}$, $\hat{\Delta} Q_{55}^{(k)}$, $\epsilon^{(k)}$, $\delta^{(k)}$, $\gamma^{(k)}$, $\epsilon_Q^{(k)}$, $\delta_Q^{(k)}$, and $\gamma_Q^{(k)}$, where $\hat{\Delta} c_{ii}^{(k)}$ and $\hat{\Delta} Q_{ii}^{(k)}$ quantify the magnitude of property variations in the model:

$$\hat{\Delta} c_{ii}^{(k)} = \Delta c_{ii}^{(k)} / \bar{c}_{ii}\,, \tag{30}$$

$$\hat{\Delta} Q_{ii}^{(k)} = \Delta Q_{ii}^{(k)} / \bar{Q}_{ii}\,, \quad ii = 33 \text{ or } 55\,. \tag{31}$$

Here, $\bar{c}_{ii} = \dfrac{1}{N}\sum_{k=1}^{N} c_{ii}^{(k)}$ and $\bar{Q}_{ii} = \dfrac{1}{N}\sum_{k=1}^{N} Q_{ii}^{(k)}$ are the arithmetic averages of c_{ii} and Q_{ii} among all N constituents, while $\Delta c_{ii}^{(k)} = c_{ii}^{(k)} - \bar{c}_{ii}$ and $\Delta Q_{ii}^{(k)} = Q_{ii}^{(k)} - \bar{Q}_{ii}$ denote the deviations from the average values. In the approximations discussed here, the squared vertical-velocity ratio $g = \dfrac{\bar{c}_{55}}{\bar{c}_{33}}$ and the vertical attenuation ratio $g_Q = \dfrac{\bar{Q}_{33}}{\bar{Q}_{55}}$ are not treated as small parameters. It is assumed, however, that the attenuation is not uncommonly strong so that quadratic and higher-order terms in $1/Q_{ii}$ can be neglected.

The approximate effective parameters for both velocity and attenuation anisotropy are given in Appendix A. For the special case of two constituents (N=2), our velocity-anisotropy parameters become identical to those given by Bakulin (2003). In principle, the exact effective velocity-anisotropy parameters depend on all possible factors including the quality-factor matrix that describes the intrinsic attenuation. However, unless the model has extremely high attenuation with some of the quality-factor components smaller than 10, the contribution of the attenuation parameters to the effective velocity anisotropy can be ignored.

In contrast, the effective attenuation anisotropy is influenced not just by the imaginary part of the stiffness matrix (i.e., by the intrinsic attenuation and the contrasts in the attenuation parameters), but also by the real parts of the stiffnesses (i.e., by the velocity parameters) and the coupling between various factors. The second-order approximations for the effective Thomsen-style attenuation parameters can be represented as (equations A37, A43, and A15):

$$\epsilon_Q = \langle \epsilon_Q \rangle + \epsilon_Q^{\text{(is)}} + \epsilon_Q^{\text{(is-Van)}} + \epsilon_Q^{\text{(is-Qan)}} + \epsilon_Q^{\text{(Van-Qan)}}, \tag{32}$$

$$\delta_Q = \langle \delta_Q \rangle + \delta_Q^{\text{(is)}} + \delta_Q^{\text{(is-Qan)}} + \delta_Q^{\text{(Van-Qan)}} + \delta_Q^{\text{(Van)}}, \tag{33}$$

$$\gamma_Q = \langle \gamma_Q \rangle + \gamma_Q^{\text{(is)}} + \gamma_Q^{\text{(is-Van)}} + \gamma_Q^{\text{(is-Qan)}} + \gamma_Q^{\text{(Van-Qan)}}, \tag{34}$$

where $\langle \cdot \rangle$ is the first-order term equal to the volume-weighted average of the intrinsic parameter values, and the rest of the terms are quadratic (second-order) in the small parameters listed above. The superscript $^{\text{(is)}}$ refers to the contribution of the parameters $\Delta c_{ii}^{(k)}$ and $\Delta Q_{ii}^{(k)}$ ($i = 3, 5$), which quantify the heterogeneity (contrasts) of the "isotropic" quantities, while $^{\text{(Van)}}$ depends on the intrinsic velocity anisotropy. The superscripts $^{\text{(is-Van)}}$, $^{\text{(is-Qan)}}$, and $^{\text{(Van-Qan)}}$ denote the quadratic terms that represent (respectively) the coupling between the isotropic heterogeneity and intrinsic velocity anisotropy, between the isotropic heterogeneity and intrinsic attenuation anisotropy, and between the intrinsic velocity and attenuation anisotropy.

Note that there are no "Van"-terms (i.e., terms quadratic in the interval velocity-anisotropy parameters) in equation 32 for ϵ_Q and equation 34 for γ_Q. The parameter δ_Q in equation 33 does include the term $\delta_Q^{\text{(Van)}}$ but not $\delta_Q^{\text{(is-Van)}}$, which is similar to the structure of equation A32 for the velocity-anisotropy parameter δ. It is interesting that while the second-order approximations for ϵ_Q, δ_Q, and γ_Q depend on the coupling between the intrinsic attenuation anisotropy and other factors (the intrinsic velocity anisotropy and the isotropic heterogeneity), none of them contains the sole contribution of the intrinsic attenuation-anisotropy parameters (i.e., there are no terms with the superscript "Qan"). The leading (first-order) term, however, is entirely controlled by the corresponding average attenuation-anisotropy parameter.

Explicit expressions for all second-order terms are listed in Appendix A. Equations A43–A48 show that the parameter δ_Q is independent of the intrinsic-anisotropy parameters $\epsilon^{(k)}$ and $\epsilon_Q^{(k)}$; this result follows directly from the exact equation 24. In contrast, ϵ_Q is influenced by all anisotropy parameters for P-SV waves ($\epsilon^{(k)}$, $\delta^{(k)}$, $\epsilon_Q^{(k)}$, and $\delta_Q^{(k)}$) because these parameters contribute to the effective values of c_{11} and Q_{11} (equation A21).

According to equations A39, A45, and A17, the isotropic-heterogeneity terms $\epsilon_Q^{\text{(is)}}$, $\delta_Q^{\text{(is)}}$ and $\gamma_Q^{\text{(is)}}$ vanish when both $c_{55}^{(k)}$ and $Q_{55}^{(k)}$ are constant for all constituents. This is a generalization of the well-known result for the effective velocity anisotropy of elastic media (Postma, 1955; Bakulin, 2003): the heterogeneity terms $\epsilon^{\text{(is)}} = \delta^{\text{(is)}} = \gamma^{\text{(is)}} = 0$ if $c_{55}^{(k)} = const$, $k = 1 \cdots N$.

As also pointed out by Bakulin (2003), $\delta^{\text{(is)}}$ in equation A34 vanishes if the vertical velocity ratio $V_{P0}^{(k)}/V_{S0}^{(k)}$ is constant for all constituents (i.e., $c_{55}^{(k)}/c_{33}^{(k)} = const$, $k = 1 \cdots N$), which means $\hat{\Delta} c_{55}/\bar{c}_{55} = \hat{\Delta} c_{33}/\bar{c}_{33}$. The parameter $\delta_Q^{\text{(is)}}$ in equation A45, however, does not preserve such a property: Even if $\hat{\Delta} c_{55}/\bar{c}_{55} = \hat{\Delta} c_{33}/\bar{c}_{33}$ and $\hat{\Delta} Q_{55}/\bar{Q}_{55} = \hat{\Delta} Q_{33}/\bar{Q}_{33}$, $\delta_Q^{\text{(is)}}$ is not zero unless $\bar{g}_Q = 1$, which means identical quality factors for all constituents ($Q_{33}^{(k)} = Q_{55}^{(k)}$, $k = 1 \cdots N$).

3.3 Velocity contrast versus attenuation contrast

As extensively discussed in the literature, velocity contrasts between thin layers cause effective velocity anisotropy in the long-wavelength limit (e.g., Backus, 1962; Brittan et al., 1995; Werner and Shapiro, 1999). The nature of the contribution of the velocity contrasts to the effective attenuation anisotropy, however, is much less obvious. In this section, we compare the influence of the velocity and attenuation contrasts on the effective attenuation-anisotropy parameters.

The second-order approximations help to separate the contributions of the velocity parameters from those of the attenuation contrasts and intrinsic attenuation anisotropy. Indeed, the attenuation-anisotropy parameters ϵ_Q and δ_Q (equations A37–A42 and A43–A48) contain several terms controlled entirely by the contrasts in the real-valued stiffnesses c_{33} and c_{55} and by the intrinsic velocity anisotropy. For example, the approximate ϵ_Q depends on $\dfrac{\Delta c_{33}^{(k,l)}}{\bar{c}_{33}} \dfrac{\Delta c_{55}^{(k,l)}}{\bar{c}_{55}}$ and $\left(\dfrac{\Delta c_{55}^{(k,l)}}{\bar{c}_{55}} \right)^2$ (see equation A39; k and l denote different constituents), as well as on $\dfrac{\Delta c_{55}^{(k,l)}}{\bar{c}_{55}} \Delta \delta^{(k,l)}$ (equation A40). This means that the velocity parameters can create effective attenuation anisotropy for P- and SV-waves even without any attenuation contrasts or intrinsic attenuation anisotropy. Still, for the attenuation-anisotropy parameters to have finite values, the constituents need to be attenuative. If the medium is purely elastic and all intrinsic Q_{ij} components are infinite, the parameters ϵ_Q, δ_Q, and γ_Q become undefined (equations 23–25).

To explore this issue further, let us consider the analytical expressions for the effective quality factor components for a medium composed of constituents with the isotropic normalized attenuation coefficient $\mathcal{A}$, in which $\epsilon_Q^{(k)} = \delta_Q^{(k)} = \gamma_Q^{(k)} = 0$ for all k. The quality-factor matrix for each constituent is described by two independent components (Carcione, 2001; Zhu and Tsvankin, 2006), which we assume to be constant for the whole model: $Q_{11}^{(k)} = Q_{33}^{(k)} \equiv Q_P$ and $Q_{55}^{(k)} = Q_{66}^{(k)} \equiv Q_S$, where

Q_P and Q_S are the quality factors for P- and S-waves, respectively. Then, as discussed by Zhu and Tsvankin (2006), the normalized attenuation coefficients in all layers will be identical and isotropic (independent of angle). Note that if the real-valued stiffnesses vary among the constituents, the quality-factor component $Q_{13}^{(k)}$ (unlike Q_P and Q_S) will not necessarily be constant. According to the definition of δ_Q (equation 24), $Q_{13}^{(k)}$ is given by

$$Q_{13}^{(k)} = Q_P \bigg/ \left[1 - \frac{(g_Q - 1)c_{55}^{(k)}(c_{13}^{(k)} + c_{33}^{(k)})^2}{2c_{13}^{(k)}(c_{13}^{(k)} + c_{55}^{(k)})(c_{33}^{(k)} - c_{55}^{(k)})}\right] , \quad (35)$$

where $g_Q \equiv Q_P/Q_S$.

The effective Q_{ij} components for this model can be obtained from equations A21–A23, A2, and A5:

$$Q_{11} = Q_P \,\mathcal{F}\left(c_{11}^{(k)}, c_{33}^{(k)}, \xi^{(k)}, \xi_Q^{(k)}\right) , \quad (36)$$

$$Q_{33} = Q_P , \quad (37)$$

$$Q_{55} = Q_{66} = Q_S , \quad (38)$$

and

$$Q_{13} = Q_P \frac{\sum_{k=1}^{N} \phi^{(k)} \xi^{(k)}}{\sum_{k=1}^{N} \phi^{(k)} \xi^{(k)} \xi_Q^{(k)}} , \quad (39)$$

where $\xi^{(k)} \equiv c_{13}^{(k)}/c_{33}^{(k)}$ and $\xi_Q^{(k)} \equiv Q_P/Q_{13}^{(k)}$. Since the expression for Q_{11} is rather lengthy, we omit the explicit form of the function $\mathcal{F}$.

Although the attenuation of all constituents is identical and isotropic, the dependence of Q_{11} and Q_{13} on the real-valued stiffnesses makes the effective attenuation for P- and SV-waves angle-dependent (i.e., $\epsilon_Q \neq 0$ and $\delta_Q \neq 0$). The normalized attenuation coefficient of SH-waves, however, is isotropic because the effective parameter γ_Q goes to zero.

For the special case of equal quality factors for P- and S-waves ($Q_P = Q_S$ and $g_Q = 1$), the element Q_{13} is constant for all constituents ($Q_{13}^{(k)} = Q_P$), and $\xi_Q^{(k)} \equiv 1$. Then $\epsilon_Q = 0$ and $\delta_Q = 0$ because all effective quality-factor components are identical ($Q_{11} = Q_{33} = Q_{13} = Q_{55} = Q_{66}$). This means that for $Q_P = Q_S$ the effective attenuation is isotropic no matter how significant are the velocity contrasts and intrinsic velocity anisotropy.

The magnitude of the velocity-induced attenuation anisotropy for a two-constituent model is illustrated in Figure 1. Both constituents have isotropic velocity functions and the same isotropic attenuation (with $Q_{33} \neq Q_{55}$). The substantial contrasts in the P- and S-wave velocities, however, create non-negligible velocity and attenuation anisotropy for P- and SV-waves. In particular, the parameter ϵ_Q reaches values close to 0.1 when the volume fractions of the constituents are equal to each other.

Next, we analyze the influence of the attenuation contrasts on the effective attenuation anisotropy by assuming that the velocity field is homogeneous and all five velocity parameters are constant: $\hat{\Delta} c_{33}^{(k)} = \hat{\Delta} c_{55}^{(k)} = 0$ and $\Delta\epsilon^{(k)} = \Delta\delta^{(k)} = \Delta\gamma^{(k)} = 0$ for all constituents k. The effective quality-factor components then have the same form:

$$Q_{ij} = \frac{1}{\sum_{k=1}^{N} \phi^{(k)}/Q_{ij}^{(k)}} , \quad (40)$$

where $ij = 11$, 33, 13, 55, or 66. When the intrinsic attenuation is isotropic (i.e., $\epsilon_Q^{(k)} = \delta_Q^{(k)} = \gamma_Q^{(k)} = 0$), the only quantities that vary among the constituents are $Q_{33}^{(k)}$ and $Q_{55}^{(k)}$. Since for isotropic intrinsic attenuation $Q_{11}^{(k)} = Q_{33}^{(k)}$ and $Q_{55}^{(k)} = Q_{66}^{(k)}$, the effective parameters ϵ_Q and $\gamma_Q = 0$ vanish. Also, the element $Q_{13}^{(k)}$ becomes

$$Q_{13}^{(k)} = \frac{Q_{33}^{(k)}}{1 - \frac{c_{55}(c_{13} + c_{33})^2}{2c_{13}(c_{13} + c_{55})(c_{33} - c_{55})}\left(\frac{Q_{33}^{(k)}}{Q_{55}^{(k)}} - 1\right)} , \quad (41)$$

where $c_{ij}^{(k)} = c_{ij}$ because the velocity field is homogeneous. The effective Q_{13} component is then given by

$$Q_{13} = \frac{Q_{33}}{1 - \frac{c_{55}(c_{13} + c_{33})^2}{2c_{13}(c_{13} + c_{55})(c_{33} - c_{55})}\left(\frac{Q_{33}}{Q_{55}} - 1\right)} . \quad (42)$$

Substituting equations 40 and 42 into equation 24 yields $\delta_Q = 0$. Hence, if the velocity field is homogeneous, the contrasts in isotropic attenuation do not produce effective attenuation anisotropy.

This conclusion is supported by the 2D finite-difference simulation of SH-wave propagation in Figure 2. The model is made up of two VTI constituents with the thicknesses less than 1/20 of the predominant wavelength, so the medium can be characterized as effectively homogeneous. Both constituents have isotropic attenuation and the same VTI velocity parameters, but there is a large contrast in the SH-wave quality-factor component Q_{55}. A snapshot of the SH-wavefront from a point source located at the center of the model is shown in Figure 2a. As pointed out by Tsvankin (2005), for 2D elastic TI models the amplitude along the SH-wavefront is constant (see the dashed circle in Figure 2b). Therefore, if the effective attenuation is directionally dependent, it should cause a deviation of the picked amplitude from a circle. However, despite some distortions produced by the automatic picking procedure, the amplitude variation along the wavefront in the attenuative model is almost negligible (Figure 2b). Clearly, the attenuation contrast does not result in effective attenuation anisotropy if it is not accompanied by a velocity contrast.

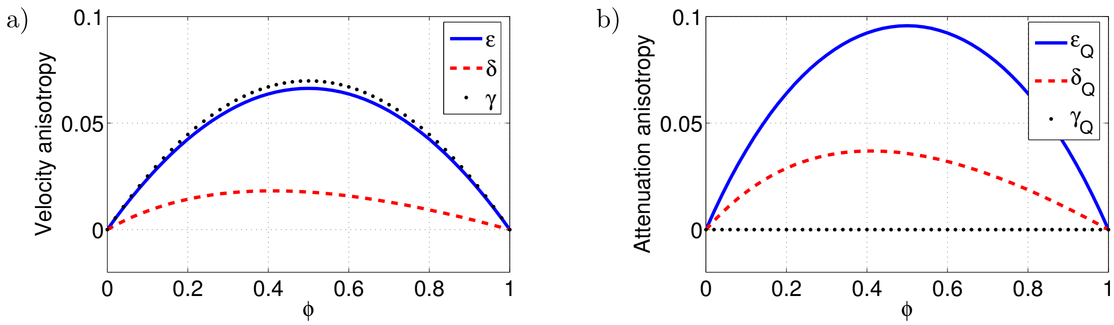

Figure 1. Exact effective anisotropy parameters computed from equations 20-25 for a layered model composed of two constituents with identical isotropic attenuation ($Q_{33}^{(1)} = Q_{33}^{(2)} = 100$; $Q_{55}^{(1)} = Q_{55}^{(2)} = 50$) and different isotropic velocity functions. The velocity contrasts are defined by $\Delta c_{33}/\bar{c}_{33} = 90\%$ and $\Delta c_{55}/\bar{c}_{55} = 70\%$; for the first constituent, $V_{P0}^{(1)} = 3.2$ km/s, $V_{S0}^{(1)} = 1.55$ km/s, and $\rho^{(1)} = 2.45\,\mathrm{g/cm}^3$. The horizontal axis represents the volume fraction of the first constituent ($\phi = \phi_1$).

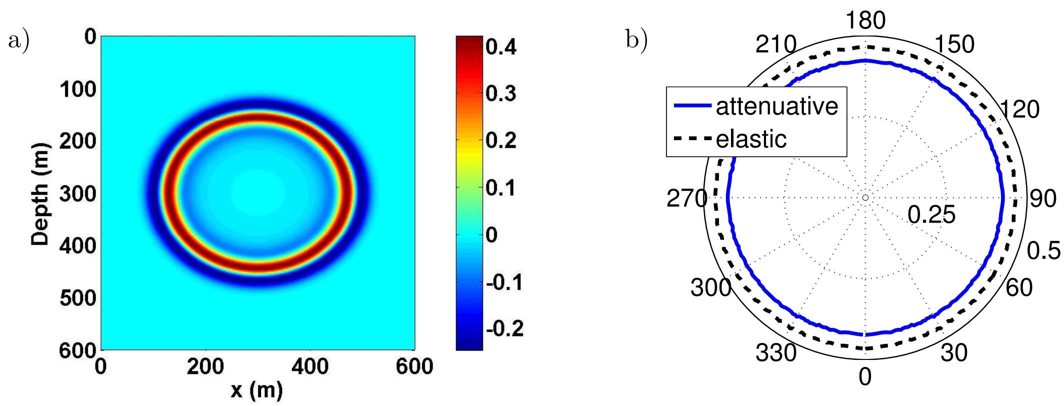

Figure 2. a) Snapshot of the SH-wavefront computed by 2D finite differences for a layered attenuative medium (the time t=0.3 s). The model includes two constituents with the same VTI velocity parameters and density: $V_S = 1500$ m/s, $\gamma = 0.2$, and $\rho = 2400$ kg/m^3. The intrinsic attenuation is isotropic; for the first constituent, $Q_{55} = Q_{66} = 20$ and the volume percentage $\phi = 33.3\%$; for the second constituent, $Q_{55} = Q_{66} = 50$. b) Polar plot of the picked amplitude along the wavefront (solid curve) and the corresponding amplitude for the elastic model with $Q_{55} = Q_{66} = \infty$ (dashed curve).

4 ACCURACY OF THE APPROXIMATIONS

To test the accuracy of the approximations introduced above, we first use a model formed by two VTI constituent layers. The velocity parameters listed in Table 1 are taken from Bakulin (2003). The maximum magnitude of the velocity-anisotropy parameters is 0.25, while the contrast in c_{33} and c_{55} reaches 30%. Since the strength of attenuation anisotropy often exceeds that of velocity anisotropy, we take each attenuation-anisotropy parameter to be twice as large by absolute value as the corresponding velocity parameter (e.g., $|\epsilon_Q| = |2\epsilon|$). Also, in accordance with the experimental results of Zhu et al. (2006), all attenuation-anisotropy parameters are negative. The contrast in the quality-factor elements Q_{33} and Q_{55} (60%) is also twice that in c_{33} and c_{55}, which means that the value of Q_{33} for the second constituent is nearly doubled compared to that for the first constituent, while Q_{55} is almost halved.

The numerical results in Figure 3 demonstrate that the linear (first-order) approximation (dashed lines) generally follows the trend of the exact effective parameters (solid lines). The maximum error for the velocity-anisotropy parameters, which occurs when the constituents occupy nearly equal volumes ($\phi = \phi^{(1)} \approx 0.5$), does not exceed 0.03. The accuracy of the linear approximation is much smaller for the attenuation-anisotropy parameters, especially for δ_Q. The error in δ_Q reaches 0.3, and the linear solution even predicts the wrong sign of this parameter for a wide range of the volume ratios ($0.3 < \phi < 1$).

Despite the substantial velocity and attenuation contrast between the two constituents, the second-order approximations in Figure 3 (dotted lines) are sufficiently

$\frac{\Delta c_{33}}{\bar{c}_{33}}$	$\frac{\Delta c_{55}}{\bar{c}_{55}}$	$\epsilon^{(1)}$	$\epsilon^{(2)}$	$\delta^{(1)}$	$\delta^{(2)}$	$\gamma^{(1)}$	$\gamma^{(2)}$
30%	−30%	0.05	0.25	0	0.2	0.05	0.25
$\frac{\Delta Q_{33}}{\bar{Q}_{33}}$	$\frac{\Delta Q_{55}}{\bar{Q}_{55}}$	$\epsilon_Q^{(1)}$	$\epsilon_Q^{(2)}$	$\delta_Q^{(1)}$	$\delta_Q^{(2)}$	$\gamma_Q^{(1)}$	$\gamma_Q^{(2)}$
60%	−60%	-0.1	-0.5	0	-0.4	-0.1	-0.5

Table 1. Parameters of a two-constituent attenuative VTI model. For the first constituent, $V_{P0} = 3$ km/s, $V_{S0} = 1.5$ km/s, $\rho = 2.4$ g/cm^3, $Q_{33} = 100$, and $Q_{55} = 80$.

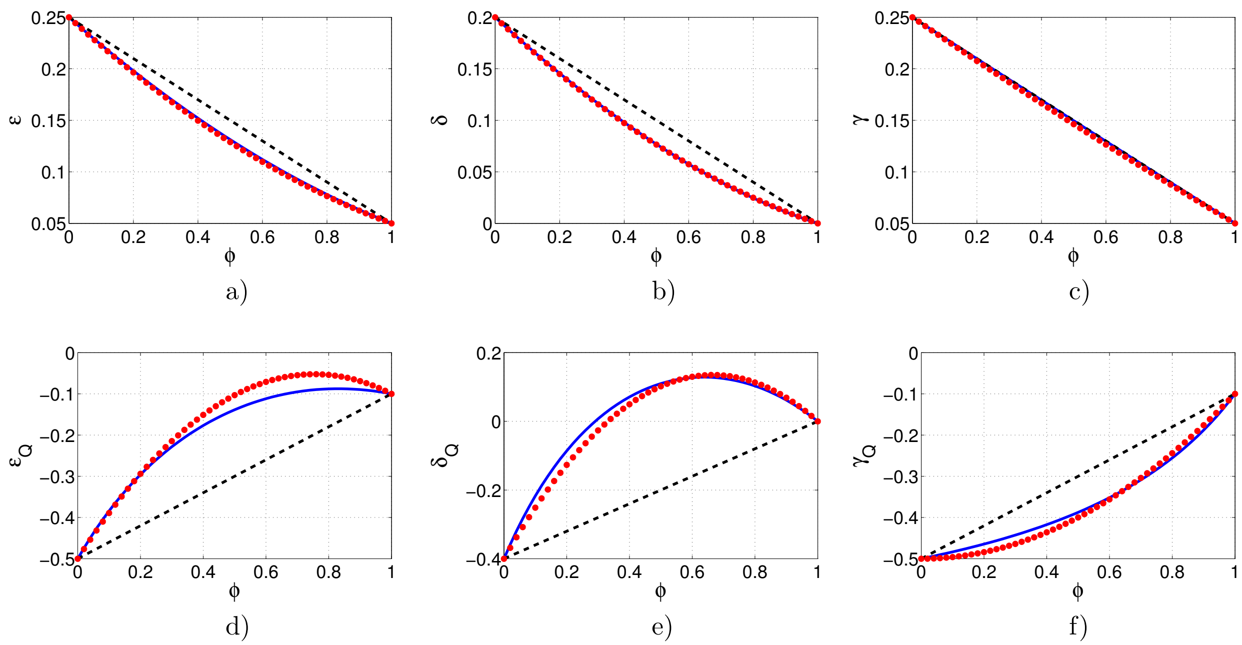

Figure 3. Effective velocity-anisotropy (a-c) and attenuation-anisotropy (d-f) parameters for the two-constituent VTI model from Table 1. The horizontal axis represents the volume fraction of the first constituent ($\phi = \phi_1$). The exact parameters (solid lines) are plotted along with the first-order linear approximations (dashed) and the second-order approximations (dotted).

close to the exact values. The maximum error does not exceed 0.005 for the velocity-anisotropy parameters and 0.04 for the attenuation-anisotropy parameters.

Next, to analyze the relative contribution of the attenuation parameters to the effective attenuation anisotropy, we change the model by making the velocity functions of both constituents isotropic and eliminating the velocity contrast between them. In agreement with the theoretical analysis in the previous section, the second-order terms for such a model become much smaller, which substantially increases the accuracy of the linear approximation (Figure 4). The only remaining second-order terms for this model are related to the coupling between the attenuation contrasts and intrinsic attenuation anisotropy.

The second-order solution for all parameters in Figure 4 virtually coincides with the exact result, which indicates that the accuracy of this approximation is mostly governed by the velocity contrasts and intrinsic velocity anisotropy. This is further confirmed by the test in Figure 5, which shows that the error of the second-order approximation remains practically negligible even for large absolute values of the attenuation-anisotropy parameters, as long as the velocity field is homogeneous and isotropic.

While the second-order approximation is adequate for a wide range of typical subsurface models, it deteriorates for uncommonly large velocity and attenuation contrasts (Figure 6). The error is particularly significant for the parameter ϵ_Q because the second-order solution produces distorted values of the quality-factor element Q_{11}.

To test the performance of our approximations for a more complicated, multi-constituent medium, we gen-

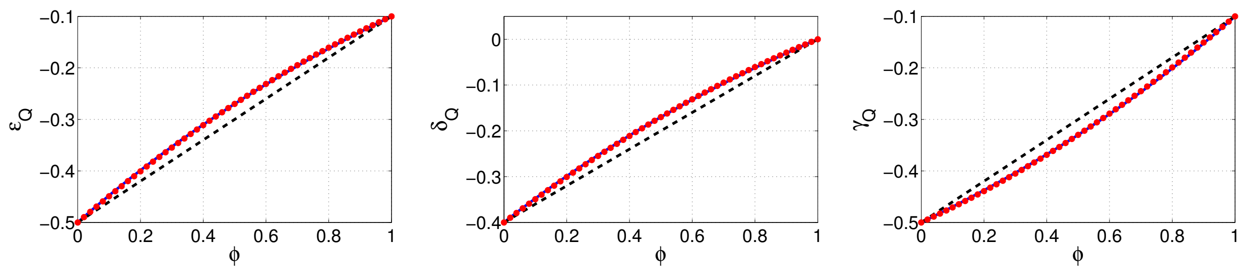

a) b) c)

Figure 4. Effective attenuation anisotropy for a model with the same attenuation parameters as those in Figure 3, but both constituents have identical isotropic velocity functions ($\epsilon^{(1)} = \epsilon^{(2)} = \delta^{(1)} = \delta^{(2)} = \gamma^{(1)} = \gamma^{(2)} = \Delta c_{33}/\bar{c}_{33} = \Delta c_{55}/\bar{c}_{55} = 0$). Compare with Figures 3d,e,f.

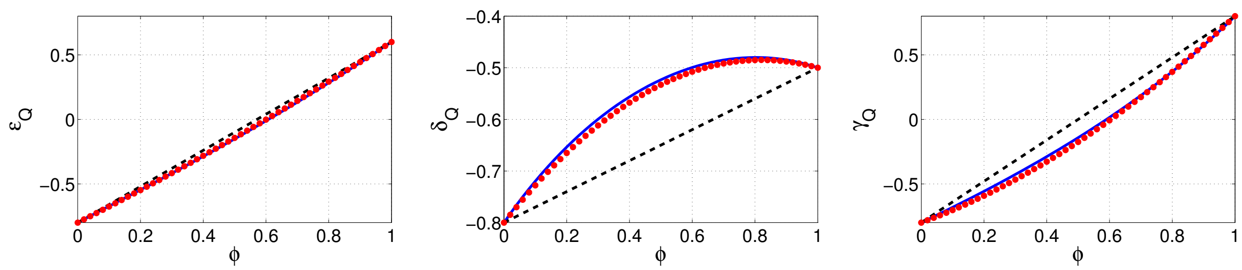

a) b) c)

Figure 5. Effective attenuation anisotropy for a model with the same velocity parameters and contrasts in Q_{33} and Q_{55} as those in Figure 3, but the intrinsic attenuation anisotropy is more pronounced: $\epsilon_Q^{(1)} = 0.6$, $\epsilon_Q^{(2)} = -0.8$, $\delta_Q^{(1)} = -0.5$, $\delta_Q^{(2)} = -0.8$, $\gamma_Q^{(1)} = 0.8$, and $\gamma_Q^{(2)} = -0.8$. As before, the exact parameters (solid lines) are plotted along with the first-order linear approximations (dashed) and the second-order approximations (dotted).

erate multiple realizations of a layered VTI model with intrinsic VTI attenuation (Figure 7). The vertical velocities (V_{P0} and V_{S0}) are computed using the $1/f^{\alpha}$ distribution with $\alpha = 0.3$. The vertical Q components Q_{33} varies between 70 and 125, while Q_{55} varies between 40 and 90. The density and interval anisotropy parameters follow normal random distributions with the following mean values: $\bar{\rho} = 2.49$ g/cm^3, $\bar{\epsilon} = 0.2$, $\bar{\delta} = 0.08$, $\bar{\gamma} = 0.15$, $\bar{\epsilon}_Q = -0.4$, $\bar{\delta}_Q = -0.16$ and $\bar{\gamma}_Q = -0.3$. The standard deviations are std(ρ) = 20 kg/m^3, std(ϵ) = std(δ) = std(γ) = 0.09, and std(ϵ_Q) = std(δ_Q) = std(γ_Q) = 0.2.

This model is similar to the one used by Bakulin and Grechka (2003), who show that the first-order (linear) approximation is surprisingly accurate for the effective velocity-anisotropy parameters of typical layered media with moderate intrinsic anisotropy. In other words, the effective velocity anisotropy is primarily determined by the mean values of the interval parameters ϵ, δ, and γ.

The test in Figure 8 demonstrates that this result also applies to effective attenuation anisotropy. After computing the exact effective parameters for 2000 realizations of the model, we can compare their ranges (bars) with the mean values (crosses) listed above. Although some of the mean values are biased, they give a generally good prediction of the effective parameters. Therefore, despite the substantial property contrasts in the model realizations, the magnitude of the second-order terms in such multiconstituent models with random parameter distributions is relatively small, and all velocity- and attenuation-anisotropy parameters are close to the mean of the corresponding interval values.

4.1 Magnitude of attenuation anisotropy

For purposes of seismic processing and inversion, it is important to evaluate the upper and lower bounds of the parameters ϵ_Q δ_Q, and γ_Q. We start with the SH-wave parameter γ_Q, which has a relatively simple analytic representation.

If a model is composed of isotropic constituents (in terms of both velocity and attenuation), the effective attenuation anisotropy is caused just by the heterogeneity. The SH-wave effective anisotropy parameters for a

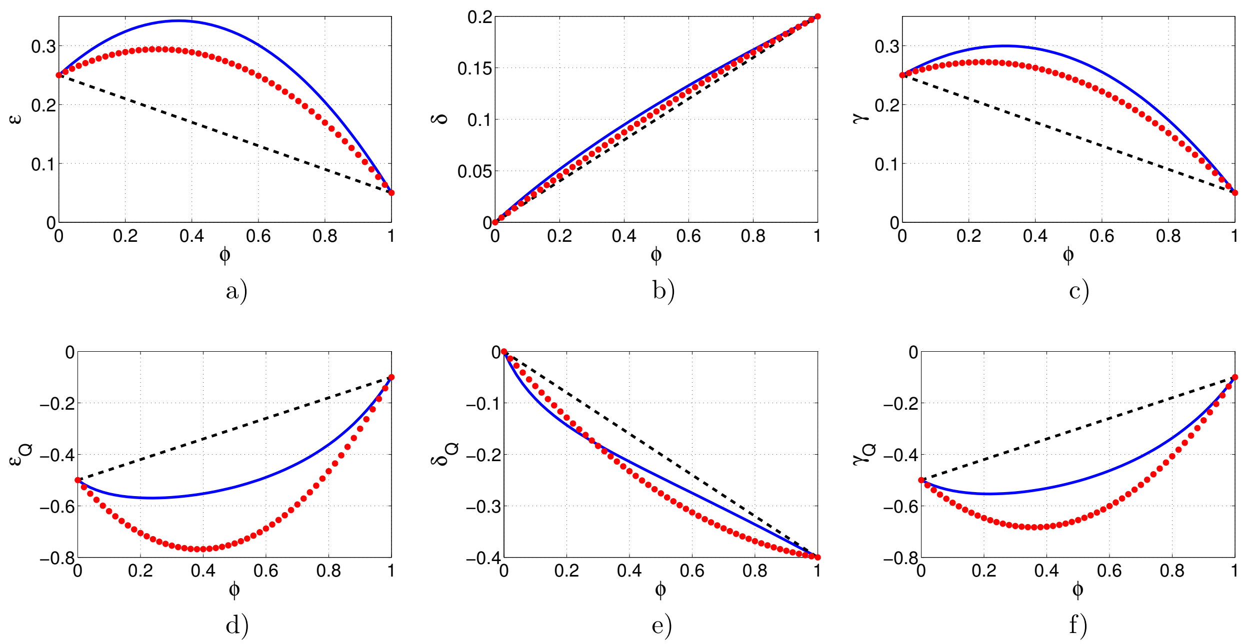

Figure 6. Effective velocity-anisotropy (a-c) and attenuation-anisotropy (d-f) parameters for a model with the same values of $\epsilon^{(1,2)}$, $\delta^{(1,2)}$, $\gamma^{(1,2)}$, $\epsilon_Q^{(1,2)}$, $\delta_Q^{(1,2)}$, and $\gamma_Q^{(1,2)}$ as those in Figure 3 (Table 1), but for much higher contrasts in the stiffnesses: $\Delta c_{33}/\bar{c}_{33} = \Delta Q_{33}/\bar{Q}_{33} = 90\%$ and $\Delta c_{55}/\bar{c}_{55} = \Delta Q_{55}/\bar{Q}_{55} = 70\%$. For the first constituent, $V_{P0}^{(1)} = 3.2$ km/s, $V_{S0}^{(1)} = 1.55$ km/s, $\rho^{(1)} = 2.45$ g/cm^3, $Q_{33}^{(1)} = 100$, and $Q_{55}^{(1)} = 80$. The exact parameters (solid lines) are plotted along with the first-order linear approximations (dashed) and the second-order approximations (dotted).

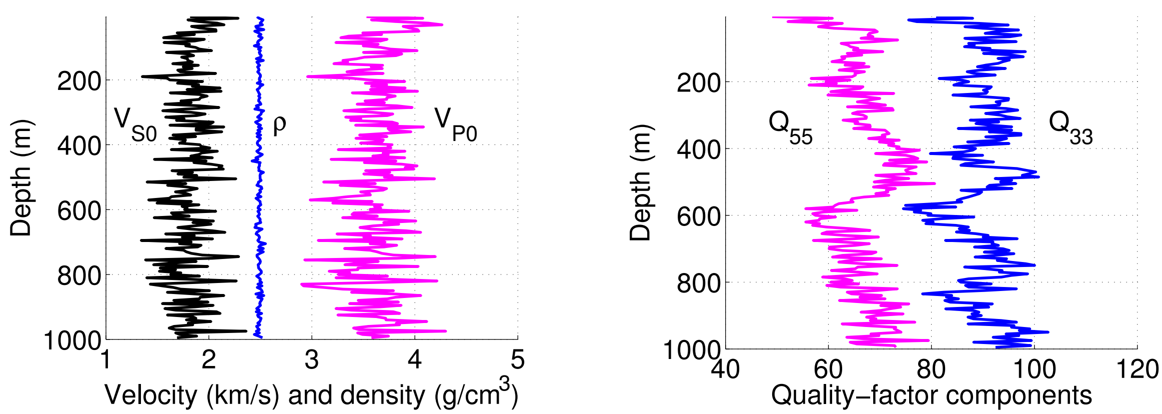

Figure 7. Vertical velocities, density, and the quality-factor components Q_{33} and Q_{55} of one realization of a model composed of VTI layers with VTI attenuation. The sampling interval is 5 m.

two-constituent isotropic model are given by

$$\gamma = 2\phi\,(1-\phi)\,\frac{x^2}{1-x^2}\,, \tag{43}$$

$$\begin{aligned}\gamma_Q = &-8\phi\,(1-\phi)\,x x_Q \\ &/[\phi(1+x)(1+x_Q) + (1-\phi)(1-x)(1-x_Q)] \\ &/[\phi(1-x) + (1-\phi)(1+x)]\,,\end{aligned} \tag{44}$$

where ϕ is the volume fraction of the first constituent, while $x \equiv (c_{55}^{(2)} - c_{55}^{(1)})/(c_{55}^{(2)} + c_{55}^{(1)})$ and $x_Q \equiv (Q_{55}^{(2)} - Q_{55}^{(1)})/(Q_{55}^{(2)} + Q_{55}^{(1)})$ denote the property contrasts between the constituents. In agreement with the discussion above, equation 44 shows that a contrast in the attenuation parameter Q_{55} is not sufficient to produce attenuation anisotropy. The parameter γ_Q also vanishes if the velocity contrast is not accompanied by an atten-

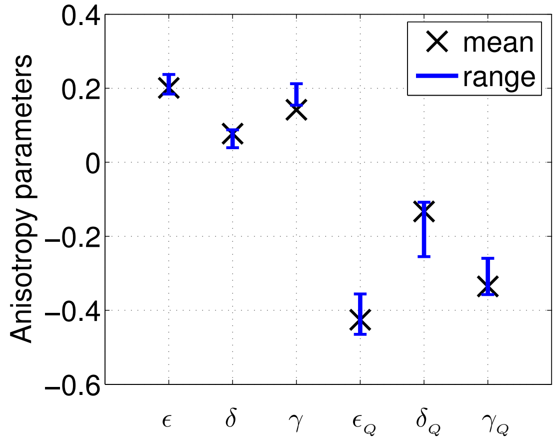

Figure 8. Mean values (crosses) of the interval anisotropy parameters and ranges (bars) of the exact effective parameters computed for 2000 realizations of the model from Figure 7. The standard deviations of all model parameters are listed in the text.

uation contrast, which is not the case for the parameters ϵ_Q and δ_Q.

It is clear from equation 43 that the velocity parameter γ is always positive and finite for layered media composed of two different isotropic constituents. This result remains valid for any number of constituents. The possible range of values of γ_Q is not immediately obvious from equation 44. For the special case $\phi = 50\%$, γ_Q has to be greater than -1, but this lower bound directly follows from the definition of the parameters γ_Q and ϵ_Q (Zhu and Tsvankin, 2006). It is difficult to estimate the upper and lower bounds of the parameter δ_Q analytically even for the simple two-constituent model.

Therefore, to study the distribution of the effective parameters for a representative set of more complicated models composed of multiple isotropic (for both velocity and attenuation) constituents, we perform numerical simulations. First, we compute the anisotropy parameters of 2000 models using uniform random distributions for the interval velocities and density. The histograms of the effective anisotropy parameters for a relatively small number of constituents (two to five) are displayed in Figure 9. As expected, the velocity-anisotropy parameters ϵ and γ are predominantly positive with the exception of a few realizations, and generally do not exceed 0.5. Another velocity-anisotropy parameter, δ, can be either positive or negative with the mean value close to zero. This is consistent with the results of Monte Carlo simulations that positive and negative δ are equally likely for finely layered media (Berryman et al., 1999). In contrast to ϵ and γ, all three effective attenuation-anisotropy parameters have an almost even distribution around the zero value and a much wider variation. For example, δ_Q can take large negative values approaching -2. However, the vast majority of the attenuation-anisotropy parameters fall within the range [-1,1].

In the next simulation (Figure 10), the maximum number of constituents is increased to 200 (the minimum number is still two). The most noticeable change in the histograms is a much more narrow distribution of both velocity-anisotropy and attenuation-anisotropy parameters, which suggests that the contributions of multiple random constituents partially cancel each other. As a result, the absolute values of the attenuation-anisotropy parameters do not exceed 0.5. Also, the distribution peaks of the parameters ϵ and γ (but not δ) are shifted toward positive values.

It should be emphasized that the tests described above were performed for models without intrinsic velocity or attenuation anisotropy. Our numerical analysis shows that making the constituents anisotropic not only moves the distribution peaks (especially, if the average value of the parameter is not zero), but also changes the shape of the histograms.

5 EFFECTIVE SYMMETRY FOR AZIMUTHALLY ANISOTROPIC MEDIA

The examples in the previous sections were generated for purely isotropic or VTI constituents, in which both velocity and attenuation are independent of azimuth. The effective velocity and attenuation functions in such models are also azimuthally isotropic, and the equivalent homogeneous medium has VTI symmetry.

The general averaging equations 8-13, however, hold for any symmetry of the interval stiffness matrix and can be used to study layered azimuthally anisotropic media. An interesting issue that arises for such models is whether or not the effective velocity and attenuation anisotropy have different principal symmetry directions (i.e., different azimuths of the vertical

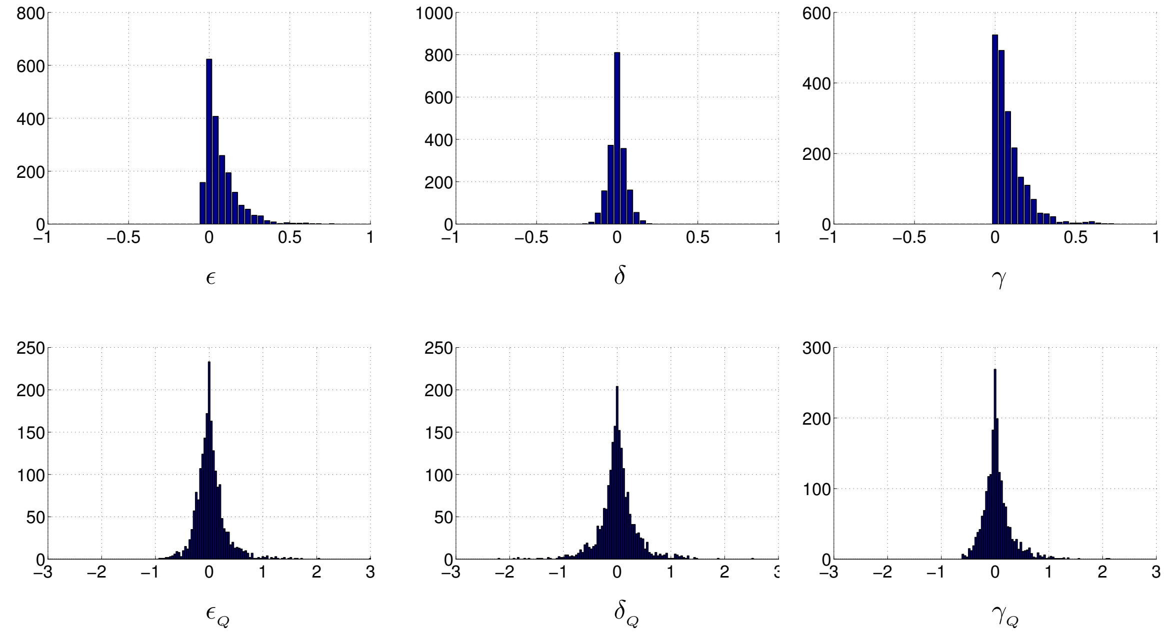

Figure 9. Histograms of the effective anisotropy parameters computed for 2000 randomly chosen models composed of isotropic (for both velocity and attenuation) constituents. The vertical axis shows the frequency of the parameter values. The ranges of the interval parameters are: $V_{P0} = 2000 - 6000$ m/s, $V_{S0} = 1000 - 3000$ m/s (the vertical P-to-SV velocity ratio was kept between 1.5 and 2.5), $\rho = 2000 - 4000$ kg/m^3, $Q_{33} = 30 - 300$, and $Q_{55} = 30 - 300$. The number of constituents is randomly chosen between two and five.

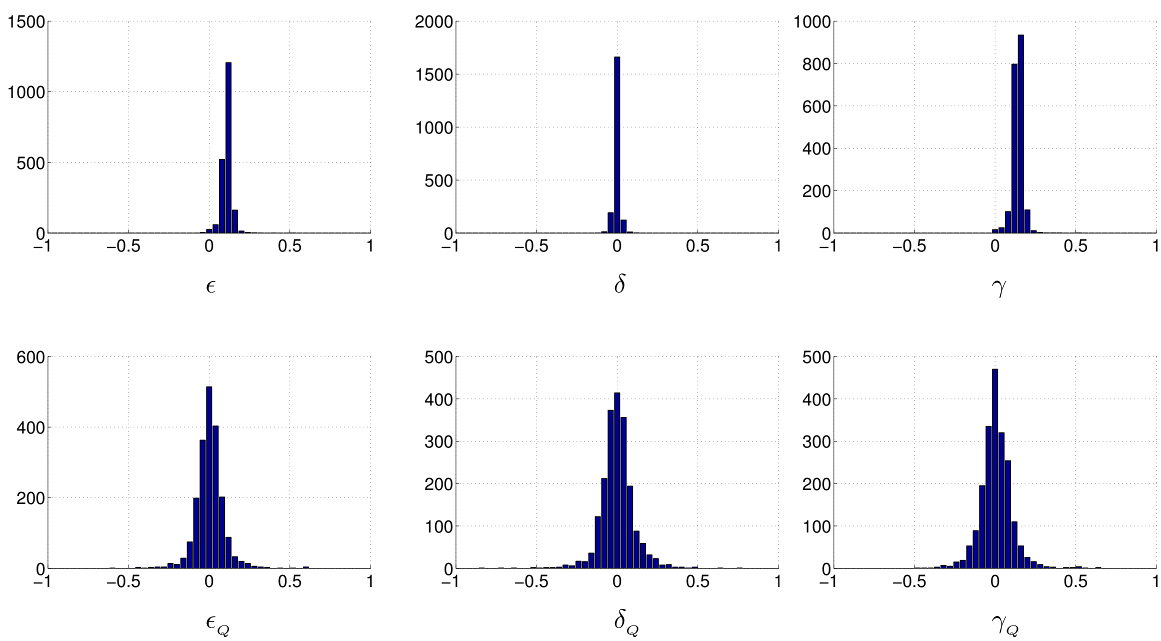

Figure 10. Same as Figure 9, but the number of constituents is randomly chosen between two and 200.

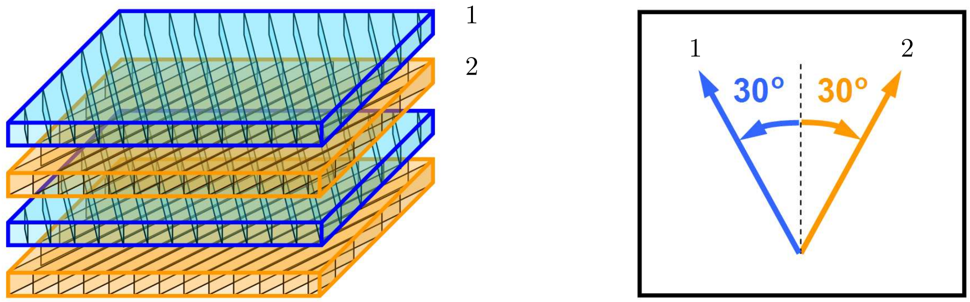

a) b)

Figure 11. a) Layered model composed of two HTI constituents with the same volume ($\phi_1 = \phi_2 = 50\%$), one of which is elastic while the other one has HTI attenuation. b) Plan view of the symmetry-plane directions. The azimuth of the symmetry plane for the first (elastic) constituent is 30° toward northwest (NW); for the second constituent, the azimuth is 30° NE. The velocity parameters for both constituents are: $\rho = 2000\,\mathrm{g/cm^3}$, $V_{P0} = 3$ km/s, $V_{S0} = 2$ km/s, $\epsilon = 0.2$, $\delta = 0.05$, and $\gamma = 0.2$. For the second constituent, the attenuation parameters are: $Q_{33}^{(2)} = 100$, $Q_{55}^{(2)} = 80$, $\epsilon_Q^{(2)} = -0.4$, $\delta_Q^{(2)} = -0.1$, and $\gamma_Q^{(2)} = -0.4$.

symmetry planes). Here, without attempting to give a comprehensive analysis of this problem, we discuss a numerical example for the simple model in Figure 11, which includes two constituents with HTI (transversely isotropic with a horizontal symmetry axis) symmetry. The first constituent is purely elastic, while the second has HTI attenuation with the same symmetry axis as that for the velocity function. The velocity parameters (i.e., the real part of the stiffness matrix) of both constituents are identical, but the symmetry axes have different orientations (Figure 11b).

The effective P-wave phase velocity and normalized attenuation coefficient $\mathcal{A}$ were computed from the Christoffel equation using the effective stiffnesses given by equations 8-13. The coefficient $\mathcal{A}$ was obtained under the assumption of homogeneous wave propagation (i.e., the planes of constant amplitude are taken to be parallel to the planes of constant phase). Since both HTI constituents in this model have identical velocity parameters and the same volume, the real part of the effective stiffness matrix should have orthorhombic symmetry. This conclusion is confirmed by the computation of the effective phase-velocity function in the horizontal plane and two vertical coordinate planes, one of which bisects (with the azimuth 90°) the symmetry-plane directions (see Figure 11). The shape of the phase-velocity curves in Figures 12a,c shows that the symmetry planes of the effective orthorhombic velocity surface are aligned with the coordinate planes.

In contrast to the velocity surface, the effective normalized attenuation coefficient is not symmetric with respect to any vertical plane (Figure 12b). Because of the coupling between the the real and imaginary parts of the effective stiffness matrix, the effective attenuation has a lower symmetry close to monoclinic. Also the extrema of the coefficient $\mathcal{A}$ in the horizontal plane do not correspond to the symmetry planes of the effective velocity surface. The minimum value of $\mathcal{A}$ occurs at an azimuth of 65°, while the maximum at 175°. Since the layering in this model is horizontal and both constituents have a horizontal symmetry axis, the monoclinic symmetry system for the effective attenuation has a horizontal symmetry plane (Figure 12d).

Next, we modify the model by reducing the magnitude of the intrinsic attenuation anisotropy ($\epsilon_Q^{(2)} = -0.1$, $\delta_Q^{(2)} = 0.03$, and $\gamma_Q^{(2)} = -0.1$; the other model parameters are the same as those in Figure 11). Since the real-values stiffnesses are kept unchanged, the effective velocity function practically coincides with that in Figures 12a,c. The horizontal and vertical cross-sections of the coefficient $\mathcal{A}$ (Figure 13) show that the effective attenuation in this model is well described by orthorhombic, rather than monoclinic, symmetry. Hence, the effective velocity and attenuation for this model have the same symmetry. Their vertical symmetry planes, however, are misaligned by about 36°.

6 DISCUSSION AND CONCLUSIONS

Interpretation of seismic amplitude measurements requires a better understanding of the physical reasons for attenuation in the seismic frequency band and, in particular, of the main factors responsible for attenuation anisotropy. Similar to velocity anisotropy, the effective attenuation coefficient can become directionally dependent due to interbedding of thin layers with different velocity and attenuation. Here, we studied the relationship between the effective Thomsen-style attenuation-anisotropy parameters (ϵ_Q, δ_Q, and γ_Q) and the properties of thin-layered media composed of attenuative isotropic or TI constituents.

The exact equations for the effective stiffness components in the long-wavelength limit were obtained us-

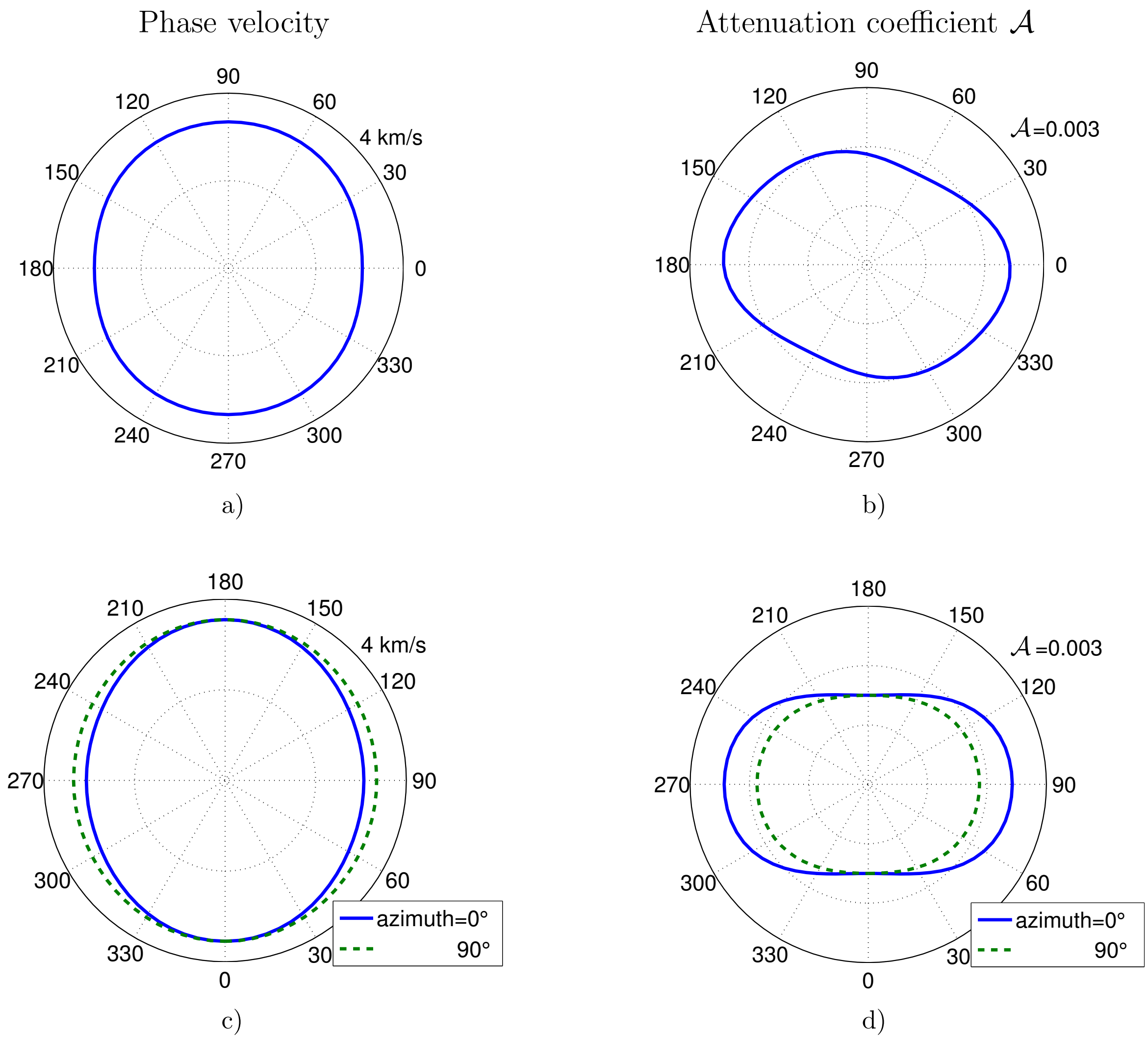

Figure 12. Effective P-wave phase velocity (left) and normalized attenuation coefficient (right) for the model from Figure 11. The velocity and attenuation are plotted in: (a,b) the horizontal plane as functions of the azimuthal phase angle; (c,d) the two vertical coordinate planes as functions of the polar phase angle.

ing the Backus averaging technique. For attenuative media, the effective stiffnesses are complex, and the attenuation anisotropy depends on both the real and imaginary parts of the stiffness matrix. In contrast, the effective velocity function is almost entirely governed by the real-valued stiffnesses and, unless the attenuation is uncommonly strong, does not depend on the intrinsic attenuation parameters. Therefore, existing results on the effective velocity anisotropy of layered media remain valid for typical attenuative subsurface models.

To gain insight into the behavior of the attenuation-anisotropy parameters for thin-layered VTI media, we developed approximate solutions by assuming that the velocity and attenuation contrasts, as well as the interval velocity- and attenuation-anisotropy parameters, are small by absolute value. As is the case for velocity anisotropy, the first-order (linear in the small quantities) term in these approximations is given simply by the volume-weighted average of the corresponding interval parameter. The second-order (quadratic) terms reflect the coupling between different factors responsible for the effective attenuation anisotropy, such as that between the intrinsic anisotropy and heterogeneity. The second-order approximation, which includes both linear and quadratic terms, remains sufficient accurate for models with strong property contrasts and pronounced intrinsic anisotropy.

It is noteworthy that even for models with isotropic constituents that have identical attenuation coefficients, the effective attenuation of P- and SV-waves is anisotropic if the interval velocity changes across layer boundaries. However, jumps in the interval attenuation

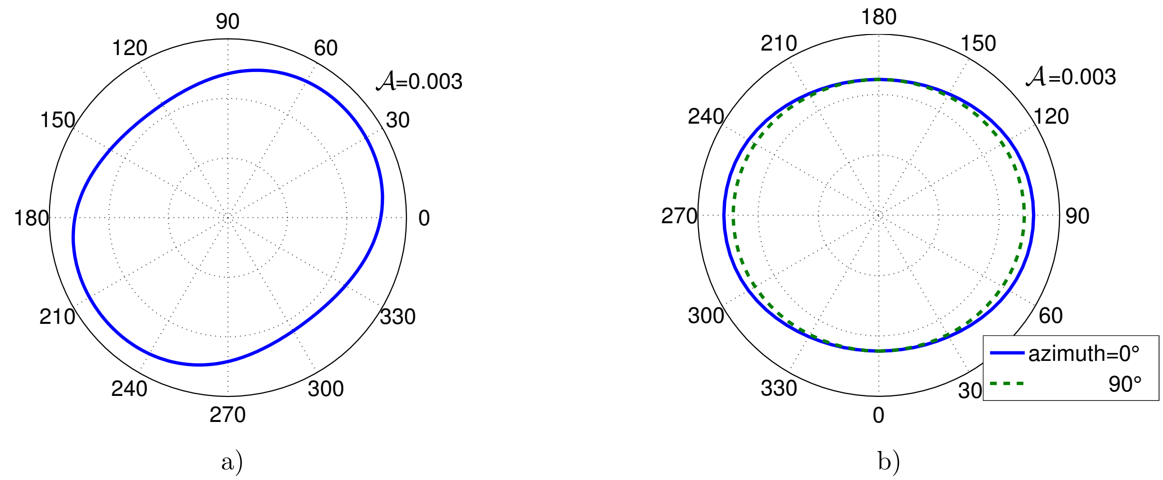

Figure 13. Horizontal (a) and vertical (b) cross-sections of the effective normalized attenuation coefficient for a model with relatively weak attenuation anisotropy. The model parameters are the same as those in Figure 11, except for $\epsilon_Q^{(2)} = -0.1$, $\delta_Q^{(2)} = 0.03$, and $\gamma_Q^{(2)} = -0.1$.

alone (i.e., not accompanied by a velocity contrast between isotropic constituent layers) do not create effective attenuation anisotropy. Because of the large contribution of the velocity contrasts to the quadratic attenuation terms, the accuracy of the linear (first-order) approximation for the attenuation-anisotropy parameters is primarily controlled by the strength of the interval velocity variations. For the same reason, the total contribution of the second-order terms tends to be higher for the attenuation parameters than for the velocity parameters. The relative magnitude of the overall velocity and attenuation anisotropy, however, is strongly dependent on the average values of the corresponding interval parameters (i.e., on the first-order term).

In addition to several tests for two-constituent models, we performed extensive numerical simulations for more complicated media composed of up to 200 constituents. To evaluate the upper and lower bounds of the attenuation anisotropy caused entirely by heterogeneity, all constituents were isotropic in terms of both velocity and attenuation. While the distributions of the parameters ϵ_Q, δ_Q, and γ_Q are centered at zero, their values cover a wider range (at least from -0.5 to 0.5) than that for the velocity-anisotropy parameters.

Although most of the paper is devoted to azimuthally isotropic models, we also evaluated the effective anisotropy for an HTI medium that includes two constituents with different azimuths of the symmetry axis. Such changes in the symmetry direction are often related to variations of the dominant fracture azimuth with depth. If the intrinsic attenuation anisotropy is sufficiently strong, the velocity and attenuation functions of the effective medium may have different symmetries (e.g., orthorhombic vs. monoclinic). Even when both velocity and attenuation are described by orthorhombic models, their vertical symmetry planes may be misaligned. These results have to be taken into account in field measurements of attenuation over fractured reservoirs.

7 ACKNOWLEDGMENTS

We are grateful to members of the A(nisotropy)-Team of the Center for Wave Phenomena (CWP), Colorado School of Mines (CSM), for helpful discussions, and to Ken Larner and Jyoti Behura (CWP) for their reviews of the manuscript. We also thank Andrey Bakulin (Shell E&P) and Ken Larner for suggesting the topic of this study. The support for this work was provided by the Consortium Project on Seismic Inverse Methods for Complex Structures at CWP and by the Chemical Sciences, Geosciences and Biosciences Division, Office of Basic Energy Sciences, U.S. Department of Energy.

REFERENCES

Arts, R. J., and P. N. J. Rasolofosaon, 1992, Approximation of velocity and attenuation in general anisotropic rocks: 62nd Annual International Meeting, Society of Exploration Geophysicists, Expanded Abstracts, 640–643.

Backus, G. E., 1962, Long wave elastic anisotropy produced by horizontal layering: Journal of Geophysical Research, **67**, 4427–4440.

Bakulin, A., 2003, Intrinsic and layer-induced vertical transverse isotropy: Geophysics, **68**, 1708–1713.

Bakulin, A., and V. Grechka, 2003, Effective anisotropy of layered media: Geophysics, **68**, 1817–1821.

Bergman, M. I., 1997, Measurements of electric anisotropy due to solidification texturing and the implications for the Earth's inner core: Nature, **389**, 60–63.

Berryman, J. G., 1979, Long-wave elastic anisotropy in transversely isotropic media: Geophysics, **44**, 896–917.

Berryman, J. G., V. Y. Grechka, and P. Berge, 1999, Analysis of Thomsen parameters for finely layered VTI media: Geophysical Prospecting, **47**, 959–978.

Bland, D., 1960, The theory of linear viscoelasticity: Pergamon Press Inc.

Brittan, J., M. Warner, and G. Pratt, 1995, Anisotropic parameters of layered media in terms of composite elastic properties: Geophysics, **60**, 1243–1248.

Carcione, J. M., 1992, Anisotropic Q and velocity dispersion of finely layered media: Geophysical Prospecting, **40**, 761–783.

Carcione, J. M., 2001, Wave fields in real media: Wave propagation in anisotropic, anelastic, and porous media: Pergamon Press.

Červený, V., and I. Pšenčík, 2005, Plane waves in viscoelastic anisotropic media – II. Numerical examples: Geophysical Journal International, **161**, 213–228.

Ferry, J. D., 1980, Viscoelastic properties of polymers: John Wiley & Sons.

Hosten, B., M. Deschamps, and B. R. Tittmann, 1987, Inhomogeneous wave generation and propagation in lossy anisotropic solids: Application to the characterization of viscoelastic composite materials: Journal of the Acoustical Society of America, **82**, 1763–1770.

Liu, E., S. Crampin, J. H. Queen, and W. D. Rizer, 1993, Velocity and attenuation anisotropy caused by microcracks and microfractures in a multiazimuth reverse VSP: Canadian Journal of Exploration Geophysics, **29**, 177–188.

Lynn, H. B., D. Campagna, K. M. Simon, and W. E. Beckham, 1999, Relationship of P-wave seismic attributes, azimuthal anisotropy, and commercial gas pay in 3-D P-wave multiazimuth data, Rulison Field, Piceance Basin, Colorado: Geophysics, **64**, 1293–1311.

Maultzsch, S., M. Chapman, E. Liu, and X. Y. Li, 2003, Modeling frequency-dependent seismic anisotropy in fluid-saturated rock with aligned fractures: implication of fracture size estimation from anisotropic measurements: Geophysical Prospecting, **51**, 381–392.

Molotkov, L.A., and A. Bakulin, 1998, Attenuation in the effective model of finely layered porous Biot media, 60th Meeting, European Association of Geoscientists and Engineers, Extended Abstracts, P156.

Pointer, T., E. Liu, and J. A. Hudson, 2000, Seismic wave propagation in cracked porous media: Geophysical Journal International, **142**, 199–231.

Postma, G. W., 1955, Wave propagation in a stratified medium: Geophysics, **XX**, 780–806.

Prasad, M., and A. Nur, 2003, Velocity and attenuation anisotropy in reservoir rocks: 73rd Annual International Meeting, Society of Exploration Geophysicists, Expanded Abstracts, 1652–1655.

Sams, M. S., 1995, Attenuation and anisotropy: The effect of extra fine layering: Geophysics, **60**, 1646–1655.

Sayers, C. M., 1994, The elastic anisotropy of shales: Journal of Geophysical Research, **99 B1**, 767–774.

Schoenberg, M., and F. Muir, 1989, A calculus for finely layered anisotropic media: Geophysics, **54**, 581–589.

Shapiro, S. A., and P. Hubral, 1996, Elastic waves in finely layered sediments: The equivalent medium and generalized Q'Doherty-Anstey formulas: Geophysics, **61**, 1282–1300.

Souriau, A., and B. Romanowicz, 1996, Anisotropy in inner core attenuation: a new type of data to constrain the nature of the solid core: Geophysical Research Letters, **23**, 1–4.

Tao, G., and M. S. King, 1990, Shear-wave velocity and Q anisotropy in rocks: A laboratory study: International Journal of Rock Mechanics and Mining Sciences and Geomechanics Abstracts, **27**, 353–361.

Thomsen, L., 1986, Weak elastic anisotropy: Geophysics, **51**, 1954–1966.

Tsvankin, I., 2005, Seismic signatures and analysis of reflection data in anisotropic media: Elsevier.

Vasconcelos, I., and E. Jenner, 2005, Estimation of azimuthally varying attenuation from surface seismic data: CWP-504, Colorado School of Mines.

Werner, U., and S. A. Shapiro, 1999, Frequency-dependent shear-wave splitting in thinly layered media with intrinsic anisotropy: Geophysics, **64**, 604–608.

Zhu, Y., and I. Tsvankin, 2006, Plane-wave propagation in attenuative TI media: Geophysics, **71**, T17–T30.

Zhu, Y., I. Tsvankin, and P. Dewangan, 2006, Physical modeling and analysis of P-wave attenuation anisotropy in transversely isotropic media: Geophysics, under review.

APPENDIX A: SECOND-ORDER APPROXIMATION FOR THE EFFECTIVE PARAMETERS OF ATTENUATIVE VTI MEDIA

Here, we derive the second-order approximation for the effective velocity- and attenuation-anisotropy parameters for thin-layered media composed of an arbitrary number of VTI (in terms of both velocity and attenuation) constituents. In accordance with the main assumption of Backus averaging (see the main text), the thickness of each layer has to be much smaller than the predominant wavelength.

A1 Anisotropy parameters for SH-waves

First, we consider the parameters γ and γ_Q, which control the velocity and attenuation anisotropy (respectively) for the SH-wave. The effective stiffness component $\tilde{c}_{55}$ is given by (see equation 17)

$$\tilde{c}_{55} = \frac{1}{\displaystyle\sum_{k=1}^{N} \frac{\phi^{(k)}}{c_{55}^{(k)}(1 - i/Q_{55}^{(k)})}}, \tag{A1}$$

where $\phi^{(k)}$ denotes the volume fraction of the k-th constituent ($\sum_{k=1}^{N} \phi^{(k)} = 1$). In the weak-attenuation limit ($\frac{1}{Q_{55}} \ll 1$), $\tilde{c}_{55}$ can be approximated as

$$\tilde{c}_{55} = \frac{\langle \frac{1}{c_{55}} \rangle - i \langle \frac{1}{c_{55} Q_{55}} \rangle}{\langle \frac{1}{c_{55}} \rangle^2}. \tag{A2}$$

From equation A2 it follows that

$$c_{55} = \langle \frac{1}{c_{55}} \rangle^{-1}, \tag{A3}$$

and

$$Q_{55} = \langle \frac{1}{c_{55}} \rangle / \langle \frac{1}{c_{55} Q_{55}} \rangle. \tag{A4}$$

According to equation 18,

$$\tilde{c}_{66} = \langle c_{66} \rangle - i \langle \frac{c_{66}}{Q_{66}} \rangle, \tag{A5}$$

which yields

$$c_{66} = \langle c_{66} \rangle, \tag{A6}$$

and

$$Q_{66} = \langle c_{66} \rangle \langle \frac{c_{66}}{Q_{66}} \rangle. \tag{A7}$$

By dropping the cubic and higher-order terms in $\hat{\Delta} c_{55}^{(k)}$ and $\gamma^{(k)}$, we obtain the second-order approximation for the effective parameter γ:

$$\gamma = \langle \gamma \rangle + \frac{1}{2} \left[\sum_{k=1}^{N} \phi^{(k)} \left(\hat{\Delta} c_{55}^{(k)} \right)^2 - \left(\sum_{k=1}^{N} \phi^{(k)} \hat{\Delta} c_{55}^{(k)} \right)^2 \right] + \left[\sum_{k=1}^{N} \phi^{(k)} \hat{\Delta} c_{55}^{(k)} \gamma^{(k)} - \sum_{k=1}^{N} \phi^{(k)} \hat{\Delta} c_{55}^{(k)} \sum_{k=1}^{N} \phi^{(k)} \gamma^{(k)} \right]. \tag{A8}$$

Note that for any quantities x and y varying among different constituents, we have

$$\sum_{k=1}^{N} \phi^{(k)} x^{(k)} y^{(k)} - \sum_{k=1}^{N} \phi^{(k)} x^{(k)} \sum_{k=1}^{N} \phi^{(k)} y^{(k)} = \sum_{k=1}^{N} \sum_{l=k+1}^{N} \phi^{(k)} \phi^{(l)} \Delta x^{(k,l)} \Delta y^{(k,l)}, \tag{A9}$$

where $\Delta x^{(k,l)} = x^{(l)} - x^{(k)}$. Then γ can be represented as

$$\gamma = \langle \gamma \rangle + \gamma^{(\text{is})} + \gamma^{(\text{is-Van})} + \gamma^{(\text{Van})}, \tag{A10}$$

where

$$\langle\gamma\rangle = \sum_{k=1}^{N} \phi^{(k)} \gamma^{(k)}\,, \tag{A11}$$

$$\gamma^{(\text{is})} = \frac{1}{2}\sum_{k=1}^{N}\sum_{l=k+1}^{N} \phi^{(k)}\phi^{(l)} \left(\frac{\Delta c_{55}^{(k,l)}}{\bar{c}_{55}}\right)^2, \tag{A12}$$

$$\gamma^{(\text{is-Van})} = \sum_{k=1}^{N}\sum_{l=k+1}^{N} \phi^{(k)}\phi^{(l)} \frac{\Delta c_{55}^{(k,l)}}{\bar{c}_{55}} \Delta\gamma^{(k,l)}\,, \tag{A13}$$

$$\gamma^{(\text{Van})} = 0\,, \tag{A14}$$

where $\Delta\cdot^{(k,l)}$ denotes the difference between the medium properties of the k-th and l-th constituents. For example, $\Delta c_{55}^{(k,l)} = c_{55}^{l} - c_{55}^{k}$ and $\Delta\gamma^{(k,l)} = \gamma^{l} - \gamma^{k}$. Equations A10-A14 generalize equations 16-19 of Bakulin (2003) for layered media with an arbitrary number of constituents.

To obtain the second-order approximation for the effective attenuation-anisotropy parameter γ_Q, we substitute equations A4 and A7 into equation 25 and keep only the linear and quadratic terms in $\hat{\Delta}c_{55}^{(k)}$, $\hat{\Delta}Q_{55}^{(k)}$, $\gamma^{(k)}$, and $\gamma_Q^{(k)}$:

$$\gamma_Q = \langle\gamma_Q\rangle + \gamma_Q^{(\text{is})} + \gamma_Q^{(\text{is-Van})} + \gamma_Q^{(\text{is-Qan})} + \gamma_Q^{(\text{Van-Qan})}\,, \tag{A15}$$

where

$$\langle\gamma_Q\rangle = \sum_{k=1}^{N} \phi^{(k)} \gamma_Q^{(k)}\,, \tag{A16}$$

$$\gamma_Q^{(\text{is})} = -2\sum_{k=1}^{N}\sum_{l=k+1}^{N} \phi^{(k)}\phi^{(l)} \frac{\Delta c_{55}^{(k,l)}}{\bar{c}_{55}} \frac{\Delta Q_{55}^{(k,l)}}{\bar{Q}_{55}}\,, \tag{A17}$$

$$\gamma_Q^{(\text{is-Van})} = -2\sum_{k=1}^{N}\sum_{l=k+1}^{N} \phi^{(k)}\phi^{(l)} \frac{\Delta Q_{55}^{(k,l)}}{\bar{Q}_{55}} \Delta\gamma^{(k,l)}\,, \tag{A18}$$

$$\gamma_Q^{(\text{is-Qan})} = \sum_{k=1}^{N}\sum_{l=k+1}^{N} \phi^{(k)}\phi^{(l)} \left(\frac{\Delta c_{55}^{(k,l)}}{\bar{c}_{55}} - \frac{\Delta Q_{55}^{(k,l)}}{\bar{Q}_{55}}\right) \Delta\gamma_Q^{(k,l)}\,, \tag{A19}$$

$$\gamma_Q^{(\text{Van-Qan})} = 2\sum_{k=1}^{N}\sum_{l=k+1}^{N} \phi^{(k)}\phi^{(l)} \Delta\gamma^{(k,l)} \Delta\gamma_Q^{(k,l)}\,. \tag{A20}$$

A2 Anisotropy parameters for P- and SV-waves

In the weak-attenuation limit, equations 14–16 yield

$$\begin{aligned}\tilde{c}_{11} = &\sum_{k=1}^{N} \phi^{(k)} c_{11}^{(k)} (1 - i/Q_{11}^{(k)}) - \sum_{k=1}^{N} \phi^{(k)} (\xi^{(k)})^2 c_{33}^{(k)} \left[1 + \frac{i}{Q_{33}^{(k)}}\left(1 - 2\,\xi_Q^{(k)}\right)\right] \\ &+ \frac{\displaystyle\sum_{k=1}^{N} \frac{\phi^{(k)}}{c_{33}^{(k)}} - i\sum_{k=1}^{N} \frac{\phi^{(k)}}{c_{33}^{(k)} Q_{33}^{(k)}}}{\displaystyle\left(\sum_{k=1}^{N} \frac{\phi^{(k)}}{c_{33}^{(k)}}\right)^2} \left\{\sum_{k=1}^{N} \phi^{(k)} \xi^{(k)} \left[1 + \frac{i}{Q_{33}^{(k)}}\left(1 - \xi_Q^{(k)}\right)\right]\right\}^2,\end{aligned} \tag{A21}$$

$$\tilde{c}_{33} = \frac{\displaystyle\sum_{k=1}^{N} \frac{\phi^{(k)}}{c_{33}^{(k)}} - i\sum_{k=1}^{N} \frac{\phi^{(k)}}{c_{33}^{(k)} Q_{33}^{(k)}}}{\displaystyle\left(\sum_{k=1}^{N} \frac{\phi^{(k)}}{c_{33}^{(k)}}\right)^2}\,, \tag{A22}$$

and

$$\tilde{c}_{13} = \frac{\sum_{k=1}^{N} \phi^{(k)} \xi^{(k)}}{\sum_{k=1}^{N} \frac{\phi^{(k)}}{c_{33}^{(k)}}} - \frac{i}{\sum_{k=1}^{N} \frac{\phi^{(k)}}{c_{33}^{(k)}}} \left[\frac{\sum_{k=1}^{N} \frac{\phi^{(k)}}{c_{33}^{(k)} Q_{33}^{(k)}}}{\sum_{k=1}^{N} \frac{\phi^{(k)}}{c_{33}^{(k)}}} \sum_{k=1}^{N} \phi^{(k)} \xi^{(k)} - \sum_{k=1}^{N} \phi^{(k)} \frac{\xi^{(k)}}{Q_{33}^{(k)}} (1 - \xi_Q^{(k)}) \right], \tag{A23}$$

where $\xi \equiv c_{13}/c_{33}$ and $\xi_Q \equiv Q_{33}/Q_{13}$. Using equation 24, ξ_Q can be rewritten as

$$\xi_Q = 1 + \frac{(1-g)\delta_Q - g(g_Q - 1)(1+\xi)^2/(1-g)}{2\xi(g+\xi)}, \tag{A24}$$

where $g \equiv \frac{c_{55}}{c_{33}}$ and $g_Q \equiv \frac{Q_{33}}{Q_{55}}$.

If we ignore the cubic and higher-order terms in δ, the second-order approximation for ξ becomes

$$\xi = 1 - 2g + \delta - \frac{\delta^2}{2(1-g)}, \tag{A25}$$

or

$$\xi = -1 - \delta + \frac{\delta^2}{2(1-g)}, \tag{A26}$$

depending on the sign of c_{13}; here, c_{13} is assumed to be positive (see equation A25).

By keeping only the linear and quadratic terms in $\hat{\Delta}c_{33}^{(k)}$, $\hat{\Delta}c_{55}^{(k)}$, $\hat{\Delta}Q_{33}^{(k)}$, $\hat{\Delta}Q_{55}^{(k)}$, as well as in the interval velocity- and attenuation-anisotropy parameters for P- and SV-waves, we obtain the second-order approximations for the effective VTI parameters.

1. Parameter ϵ:

$$\epsilon = \langle \epsilon \rangle + \epsilon^{\text{(is)}} + \epsilon^{\text{(is-Van)}} + \epsilon^{\text{(Van)}}, \tag{A27}$$

where

$$\langle \epsilon \rangle = \sum_{k=1}^{N} \phi^{(k)} \epsilon^{(k)}, \tag{A28}$$

$$\epsilon^{\text{(is)}} = 2\bar{g} \sum_{k=1}^{N} \sum_{l=k+1}^{N} \phi^{(k)} \phi^{(l)} \left[\frac{\Delta c_{33}^{(k,l)}}{\bar{c}_{33}} \frac{\Delta c_{55}^{(k,l)}}{\bar{c}_{55}} - \bar{g} \left(\frac{\Delta c_{55}^{(k,l)}}{\bar{c}_{55}} \right)^2 \right], \tag{A29}$$

$$\epsilon^{\text{(is-Van)}} = \sum_{k=1}^{N} \sum_{l=k+1}^{N} \phi^{(k)} \phi^{(l)} \frac{\Delta c_{33}^{(k,l)}}{\bar{c}_{33}} (\Delta\epsilon^{(k,l)} - \Delta\delta^{(k,l)}) + 2\bar{g} \frac{\Delta c_{55}^{(k,l)}}{\bar{c}_{55}} \Delta\delta^{(k,l)}, \tag{A30}$$

$$\epsilon^{\text{(Van)}} = -\frac{1}{2} \sum_{k=1}^{N} \sum_{l=k+1}^{N} \phi^{(k)} \phi^{(l)} \left(\Delta\delta^{(k,l)} \right)^2, \tag{A31}$$

and $\bar{g} = \frac{\bar{c}_{55}}{\bar{c}_{33}}$.

2. Parameter δ:

$$\delta = \langle \delta \rangle + \delta^{\text{(is)}} + \delta^{\text{(is-Van)}} + \delta^{\text{(Van)}}, \tag{A32}$$

where

$$\langle \delta \rangle = \sum_{k=1}^{N} \phi^{(k)} \delta^{(k)}, \tag{A33}$$

$$\delta^{\text{(is)}} = 2\bar{g} \sum_{k=1}^{N} \sum_{l=k+1}^{N} \phi^{(k)} \phi^{(l)} \left(\frac{\Delta c_{33}^{(k,l)}}{\bar{c}_{33}} - \frac{\Delta c_{55}^{(k,l)}}{\bar{c}_{55}} \right) \frac{\Delta c_{55}^{(k,l)}}{\bar{c}_{55}}, \tag{A34}$$

$$\delta^{(\text{is-Van})} = 0\,, \tag{A35}$$

$$\delta^{(\text{Van})} = -\frac{1}{2}\sum_{k=1}^{N}\sum_{l=k+1}^{N}\phi^{(k)}\phi^{(l)}\frac{\left(\Delta\delta^{(k,l)}\right)^2}{1-\bar{g}}\,. \tag{A36}$$

As was the case for SH-waves, equations A27-A36 generalize equations 29-32 and 21-24 of Bakulin (2003) for multi-constituent layered media.

3. Parameter ϵ_Q:

$$\epsilon_Q = \langle\epsilon_Q\rangle + \epsilon_Q^{(\text{is})} + \epsilon_Q^{(\text{is-Van})} + \epsilon_Q^{(\text{is-Qan})} + \epsilon_Q^{(\text{Van-Qan})}\,, \tag{A37}$$

where

$$\langle\epsilon_Q\rangle = \sum_{k=1}^{N}\phi^{(k)}\epsilon_Q^{(k)}\,, \tag{A38}$$

$$\begin{aligned}\epsilon_Q^{(\text{is})} = -4\bar{g}\sum_{k=1}^{N}\sum_{l=k+1}^{N}\phi^{(k)}\phi^{(l)} &\left[(1-\bar{g}_Q)\left(\frac{\Delta c_{33}^{(k,l)}}{\bar{c}_{33}} - 2\bar{g}\frac{\Delta c_{55}^{(k,l)}}{\bar{c}_{55}}\right)\frac{\Delta c_{55}^{(k,l)}}{\bar{c}_{55}} + \frac{\Delta c_{55}^{(k,l)}}{\bar{c}_{55}}\frac{\Delta Q_{33}^{(k,l)}}{\bar{Q}_{33}}\right.\\ &\left. +\bar{g}_Q\left(\frac{\Delta c_{33}^{(k,l)}}{\bar{c}_{33}} - 2\bar{g}\frac{\Delta c_{55}^{(k,l)}}{\bar{c}_{55}}\right)\frac{\Delta Q_{55}^{(k,l)}}{\bar{Q}_{55}}\right]\,,\end{aligned} \tag{A39}$$

$$\begin{aligned}\epsilon_Q^{(\text{is-Van})} = 2\sum_{k=1}^{N}\sum_{l=k+1}^{N}\phi^{(k)}\phi^{(l)} &\left[-2\bar{g}(1-\bar{g}_Q)\frac{\Delta c_{55}^{(k,l)}}{\bar{c}_{55}}\Delta\delta^{(k,l)} - 2\bar{g}\bar{g}_Q\frac{\Delta Q_{55}^{(k,l)}}{\bar{Q}_{55}}\Delta\delta^{(k,l)}\right.\\ &\left. -\frac{\Delta Q_{33}^{(k,l)}}{\bar{Q}_{33}}(\Delta\epsilon^{(k,l)} - \Delta\delta^{(k,l)})\right]\,,\end{aligned} \tag{A40}$$

$$\epsilon_Q^{(\text{is-Qan})} = \sum_{k=1}^{N}\sum_{l=k+1}^{N}\phi^{(k)}\phi^{(l)}\left[\frac{\Delta c_{33}^{(k,l)}}{\bar{c}_{33}}(\Delta\epsilon_Q^{(k,l)} - \Delta\delta_Q^{(k,l)}) - \frac{\Delta Q_{33}^{(k,l)}}{\bar{Q}_{33}}\Delta\epsilon_Q^{(k,l)} + 2\bar{g}\frac{\Delta c_{55}^{(k,l)}}{\bar{c}_{55}}\Delta\delta_Q^{(k,l)}\right]\,, \tag{A41}$$

$$\epsilon_Q^{(\text{Van-Qan})} = \sum_{k=1}^{N}\sum_{l=k+1}^{N}\phi^{(k)}\phi^{(l)}\left[2\Delta\epsilon^{(k,l)}\Delta\epsilon_Q^{(k,l)} - \Delta\delta^{(k,l)}\Delta\delta_Q^{(k,l)}\right]\,. \tag{A42}$$

4. Parameter δ_Q:

$$\delta_Q = \langle\delta_Q\rangle + \delta_Q^{(\text{is})} + \delta_Q^{(\text{is-Qan})} + \delta_Q^{(\text{Van-Qan})} + \delta_Q^{(\text{Van})}\,, \tag{A43}$$

where

$$\langle\delta_Q\rangle = \sum_{k=1}^{N}\phi^{(k)}\delta_Q^{(k)}\,, \tag{A44}$$

$$\begin{aligned}\delta_Q^{(\text{is})} = -4\bar{g}\sum_{k=1}^{N}\sum_{l=k+1}^{N}\phi^{(k)}\phi^{(l)} &\left[(1-\bar{g}_Q)\left(\frac{\Delta c_{33}^{(k,l)}}{\bar{c}_{33}} - \frac{\Delta c_{55}^{(k,l)}}{\bar{c}_{55}}\right)\frac{\Delta c_{55}^{(k,l)}}{\bar{c}_{55}} + \frac{\Delta c_{55}^{(k,l)}}{\bar{c}_{55}}\frac{\Delta Q_{33}^{(k,l)}}{\bar{Q}_{33}}\right.\\ &\left. +\bar{g}_Q\left(\frac{\Delta c_{33}^{(k,l)}}{\bar{c}_{33}} - 2\frac{\Delta c_{55}^{(k,l)}}{\bar{c}_{55}}\right)\frac{\Delta Q_{55}^{(k,l)}}{\bar{Q}_{55}}\right]\,,\end{aligned} \tag{A45}$$

$$\delta_Q^{(\text{is-Qan})} = -\sum_{k=1}^{N}\sum_{l=k+1}^{N}\phi^{(k)}\phi^{(l)}\frac{\Delta Q_{33}^{(k,l)}}{\bar{Q}_{33}}\Delta\delta_Q^{(k,l)}\,, \tag{A46}$$

$$\delta_Q^{(\text{Van-Qan})} = -\frac{1}{1-\bar{g}} \sum_{k=1}^{N} \sum_{l=k+1}^{N} \phi^{(k)} \phi^{(l)} \Delta\delta^{(k,l)} \Delta\delta_Q^{(k,l)} \,, \tag{A47}$$

$$\delta_Q^{(\text{Van})} = \bar{g} \frac{1-\bar{g}_Q}{(1-\bar{g})^2} \sum_{k=1}^{N} \sum_{l=k+1}^{N} \phi^{(k)} \phi^{(l)} (\Delta\delta^{(k,l)})^2 \,, \tag{A48}$$

where $\bar{g}_Q = \dfrac{\bar{Q}_{33}}{\bar{Q}_{55}}$.